Scientific Reports

https://doi.org/10.1038/s41598-026-41176-0

Article in Press

A novel bioenergetic model outlines the metabolism of a deep-sea clam and that of its sulfur-oxidizing symbionts

Received: 9 October 2025

Accepted: 18 February 2026

Published online: 21 March 2026

Cite this article as: Vandenberghe M., Marques G.M., Andersen A.C. *et al.* A novel bioenergetic model outlines the metabolism of a deep-sea clam and that of its sulfur-oxidizing symbionts. *Sci Rep* (2026). https://doi.org/10.1038/s41598-026-41176-0

Marine Vandenberghe, Gonçalo M. Marques, Ann C. Andersen, Carole Decker, Karine Olu, Sébastien Duperron & Sylvie M. Gaudron

A novel bioenergetic model outlines the metabolism of a deep-sea clam and that of its sulfur-oxidizing symbionts

Marine Vandenberghe[1], Gonçalo M. Marques[2], Ann C. Andersen[3], Carole Decker[4], Karine Olu[4], Sébastien Duperron[5], and Sylvie M. Gaudron[1,6,*]

[1]UMR 8187 Laboratoire d'Océanologie et de Géosciences (LOG), Université de Lille, ULCO, CNRS, IRD, F-59000 Lille, France
[2]Marine, Environment & Technology Center (MARETEC), LARSyS, Instituto Superior Técnico, University of Lisboa, Portugal
[3]Sorbonne Université, CNRS, Station Biologique de Roscoff, Adaptation et Diversité en Milieu Marin, AD2M, F-29680 Roscoff, France
[4]Ifremer, Laboratoire Environnement Profond, Centre Bretagne - ZI de la Pointe du Diable - CS 10070 - 29280 Plouzané, France
[5]UMR7245 Molécules de Communication et Adaptation des Microorganismes, Muséum national d'Histoire naturelle, Paris, France
[6]Sorbonne Université, UFR 927, F-75005 Paris, France
[*]sylvie.gaudron@univ-lille.fr

ABSTRACT

For the first time, two Dynamic Energy Budget (DEB) models were developed for a chemosymbiotic deep-sea vesicomyid clam. A classical DEB model was applied and then an innovative DEB model was developed (named "farming"). The models were parameterized using data on host and symbionts, including original unpublished data. In the farming model the digestion of the sulfur-oxidizing bacterial symbionts for host nutrition was explicitly modeled. Unexpected results were obtained regarding the dynamics of host and symbionts with this model: the host appears to forgo a maximal ingestion for a lower and stable ingestion, revealing a new kind of homeostasis. Moreover, when the clam is adult, most of the oxygen consumed by the chemosynthetic symbiosis was predicted to be by the symbionts. A high host energy maintenance flux was predicted and consistent with the likely high energy demand of host ion homeostasis mechanisms to cope with symbiont protons and sulfates release.

Introduction

Deep-sea chemosynthesis-based ecosystems (> 200 m depth) derive their energy from chemical compounds and not from sunlight. Examples are hydrothermal vents, cold seeps, and organic falls, in which dense communities of specialized symbiotic animals occur, including typical specialized clams, tubeworms and mussels. These species are nutritionally dependent on symbiotic relationships with chemosynthetic bacteria that use available reduced chemical compounds, such as hydrogen sulfide and/or methane, as energy sources to fix inorganic carbon and synthesize organic molecules[1].

Vesicomyidae (Mollusca, Bivalvia) are typical bivalves inhabiting various reduced habitats from the continental shelf to hadal depths worldwide[2,3]. These clams have several unique features to thrive in extreme and nutrient-poor environments, in particular their enlarged gills (compared to other bivalves of a similar size) hosting high density of sulfur-oxidizing autotrophic bacteria[2,4] and providing an important surface area for extracting oxygen and exchanging compounds with surrounding waters. In most symbiotic vesicomyid species, a single bacterial strain belonging to the Gammaproteobacteria class is highly dominant and is host-species specific[1]. Symbionts have reduced genomes compared to free-living relatives[5–9]. Bacterial symbionts were also observed in vesicomyid fully-grown oocytes[5,10,11] and around primary oocytes[12] suggesting vertical, mother-to-offspring transmission. Nonetheless, some lateral transmission of symbionts from nearby hosts may occur[4,5,13,14]. The previous elements indicate a coevolution between symbiotic vesicomyid and their major symbionts that even leads to co-speciation events between hosts and their symbionts[7,8,15].

The species *Christineconcha regab* (Vesicomyidae, Pliocardiinae) was discovered at the Regab pockmark, a cold seep located in the Gulf of Guinea (southeast Atlantic) that has been extensively explored by oil and gas companies, geologists and biologists from 1964 to 2011[16–18]. Methane was the major chemical component of the emitted fluids in this reducing deep-sea

habitat[17,19–21]. In the Gulf of Guinea, *C. regab* was observed from -2820 m depth near cold seeps to -5070 m depth at the Lobes of the Congo deep-sea fan, that are the ends of the channel-levee enriched in buried organic matter[16,20,21]. This clam was also encountered on the Bonjardim mud volcano in the Gulf of Cadiz (-3060 m depth)[22,23] and in reduced sediments in the Bay of Biscay in the Northeast Atlantic (-4125 m depth)[24]. *C. regab* lives in aggregates and about two-third of its anterior part shell is burried in sediments. It uses its highly vascularized foot to move and dig into the sediment for sulfide to sustain its sulfur-oxidizing (SOX) symbionts (Taxonomy ID: NCBI:txid1365817) and overall contribute to bioturbation[25], that favors oxygen and sulfate supply in surface sediments enhancing sulfate reduction and anaerobic oxidation of methane (AOM)[26,27]. Symbionts may acquire carbon dioxide, nitrate and dioxygen at the clam gill/seawater interface, where two-thirds of *C. regab* gill volume was shown to be occupied with these SOX bacteria[25,28]. The clam mantle and gills had depleted carbon isotopic signatures ($\delta^{13}C$ approximately -38.9 and -38.2 ‰ for mantle and gills, respectively), which were congruent with clam symbiotic nutrition[27].

The "farming" feeding strategy - where the host provides its symbionts with inorganic carbon, reduced compounds, and oxygen and then digests them to get organic matter - seems to exist in most of chemosymbioses[29]. Symbiotic vesicomyids are very likely using this farming strategy, as was suggested by the observation of lysosomes in vesicomyid bacteriocytes by transmission electron microscopy and further supported by a high expression of lysozyme genes in vesicomyid species gills[30,31]. Degradation stages of symbionts were also observed in vesicomyid bacteriocytes[32]. A fractionation of nitrogen stable isotopic values between host gills (symbiotic bacteria) and mantle tissues of vesicomyid bivalve (e.g., *C. regab*) may also indicate the preferential use of the farming feeding strategy[27]. Vesicomyids may use an additional feeding strategy called "milking" where transfer of organic carbon from the symbionts to the host occurs via organic molecules and/or via the symbiont production of outer membrane vesicles[33]. High transcription of substrate-specific transporters by symbionts and expanded transport genes in vesicomyid species indicated that milking may occur[8,32]. We cannot completely exclude that the milking strategy do not exist in vesicomyid and it should be explored in further bioenergetic model in the future but we have made the choice here to concentrate on the development of the farming strategy for this model.

Two studies have modeled the metabolic rate of the symbiotic mixotrophic deep-sea bivalve *Bathymodiolus azoricus* (Bathymodiolinae) from hydrothermal vents. This deep-sea mussel is able to filter feed and relies on its methane- and sulfur-oxidizing symbionts as food sources. In the first two models developed on *B. azoricus*, carbon consumption flux of its endosymbionts and host filtration of the particle organic matter were included[34,35]. The first model did not include the effect of temperature on metabolic rates and did not use experimental data[35]. In this model, the endosymbiont scale functional response (i.e., the term "functional response" (f) refers to the ingestion rate as a function of the food density),[36]) was defined as a Michaelis–Menten function using the concentration of either methane and sulfide as the food level. The mass of the symbionts, which represented 4% of the gill wet weight, was used but fixed[35]. The second model was an improvement of the previous model with the addition of parameters controlling the input and uptake flows, the inclusion of the symbiont biomass, and the mussel assimilation with temperature correction for metabolic rates[34].

Dynamic energy budget (DEB) theory[36] is a bioenergetic model already in use for applications with multiple species. DEB theory is an individual-based framework encompassing the whole life cycle of an organism. Processes, such as ingestion, assimilation, growth, reproduction and respiration, are quantified in terms of energy or mass fluxes forced by environmental parameters (e.g., food level and temperature). Currently, only two DEB models have been developed on deep-sea benthic invertebrate species: one for the obligate wood-feeder bivalve *Xylonora atlantica*[37] and one for the symbiotic mussel *Bathymodiolus azoricus*[38]. In the latter model, thiotrophic symbionts have been included as a flux of hydrogen sulfide assimilated by the mussel. Attempts to model host-symbionts inter relationships using DEB by explicitly incorporating the symbionts were only done on shallow marine organisms, coral-*Symbiodinium*[39] and anemone-*Symbiodinium*[40].

Symbiotic interactions and the part host and symbionts play respectively in the chemosymbiosis are still little known and hard to disentangle. In deep-sea chemosymbiosis, symbionts are the main and often the only food source of their host. Unravelling the dynamic and impact of symbionts on their host at the individual level is a first step to understand the population dynamic of such deep-sea species. This paper is the first attempt to model both symbionts and their bivalve host separately in a single framework using the DEB theory. Therefore the dynamics between the host deep-sea clam *C. regab* and its obligate sulfur-oxidizing symbionts were modelled given the preliminary hypothesis that the host feeds using only a farming strategy. SOX symbionts have been explicitly defined and incorporated within the developed farming DEB model for *C. regab*. The objectives of this paper were resumed as follows:

1. To develop an original two-species DEB model for a deep-sea symbiotic bivalve species and its SOX symbionts under the farming strategy framework;

2. To compare the bivalve host life traits and energy allocation obtained both from a classical DEB model and the new farming model;

3. To describe the dynamics of symbionts energy allocation for different sizes of host and food level at a typical cold-seep temperature;

4. To estimate and predict the chemical fluxes of carbon, oxygen and nitrogen of the vesicomyid clam host and its SOX symbionts separately at different food level and at a typical cold seep temperature.

Results

Models' calibration

Parameters of the classical and of the farming models were estimated (Supplementary Table 1). The comparison between the data inputed for the parameter estimation and the model predictions (Supplementary Figures 1 and 2, Supplementary Table 2) resulted, respectively for the classical and the farming models, in a MRE (mean relative error) of 0.094 and 0.195, a SMAE (standardized mean absolute error) of 0.053 and 0.088, and a SMSE (symmetric mean squared error) of 0.029 and 0.049 (Supplementary Table 1).

The length at hatching, birth, metamorphosis and puberty, and the lifespan were better predicted with the farming model (relative error (RE) < 0.005), whereas the clam maximum reproduction rate and ultimate length were better predicted with the classical model (RE < 0.007) (Supplementary Table 2). With the farming model, the relative errors of the carbon flux predictions were lower than with the classical model whereas with for nitrogen fluxes the classical model gave better predictions (Supplementary Table 2). For oxygen fluxes, no important differences in predictions between the two models could be assessed (Supplementary Table 2).

The symbiont-related data could only be predicted with the farming model. The ratio of the bacteria-to-gill volume was well predicted (RE ‹ 0.005; Supplementary Table 2). Symbiont yields for hydrogen sulfide assimilation were well predicted for sulfate and dioxygen (RE = 0.01 and RE = 0.33 respectively; Supplementary Table 2) whereas the yield for nitrogen was not (RE › 17; Supplementary Table 2). The yield of HS^- mol per C-mol of symbiont biomass was relatively well predicted (RE = 0.80, Supplementary Table 2) compared to the yield of symbiont biomass in g per mol of H_2S (RE = 2.79, Supplementary Table 2).

Both the classical and the farming models predicted well: the relationships between shell length and wet weight (L-Ww, Supplementary Figs. 1a (RE = 0.08–0.21) and 2a (RE = 0.09–0.28) for the classical and the farming models, respectively), between shell length and dry weight (L-Wd, Supplementary Figs. 1b (RE = 0.14–0.35) and 2b (RE = 0.13–0.41)), between reproduction rate and shell length (R-L, Supplementary Figs. 1c (RE = 0.60–7.50) and 2c (RE = 0.58–7.57)) and between reproduction rate and wet weight (R-Ww, Supplementary Figs. 1d (RE = 0.62–6.46) and 2d (RE = 0.58–5.63)). With both model, univariate data sets related to the reproduction rate were less well predicted, with data sets R-L and R-Ww from site Regab Southwest (RE > 1). RE for time-length predictions with the classical and the farming models were RE = 0.01 and RE = 0.03–0.02, respectively. The main difference between the two models lies in the estimated growth rate of the host (time-length curves, Supplementary Figs. 1e and 2e for the classical and farming models, respectively).

With the classical model, the von Bertalanffy growth coefficient ($\dot{r}_B$) was estimated at 8.3×10^{-4} d^{-1} while it was predicted 4-fold slower at 2.3×10^{-4} d^{-1} with the farming model. Using the estimated Bertalanffy growth coefficient, the *C. regab* growth rates for Regab sites were estimated to be, respectively with the classical and the farming model, 2.27 $cm\,yr^{-1}$ and 1 $cm\,yr^{-1}$, 1 day after metamorphosis (L_j); 0.67 $cm\,yr^{-1}$ and 0.72 $cm\,yr^{-1}$, 5 years after L_j; 0.08 $cm\,yr^{-1}$ and 0.4 $cm\,yr^{-1}$, 12 years after L_j.

Estimated functional responses and sensitivity analysis

With the classical model, the estimated functional responses (f) were 0.68 and 0.65 for the Regab Center and Southwest sites, respectively, and 2.2, 0.8 and 5.90 for the Lobe A, B, and C sites respectively.

With the farming model, as symbionts within gills of *C. regab* were provided experimentally with a reasonable concentration of sulfide, the symbiont functional response for sulfide consumption (f_{Ss}) was set at 0.8. This value corresponds to a high functional response for *in-situ* conditions (close to the theoretical highest 1), leaving room for a higher symbiont functional response in other environmental conditions. For the Regab Center and Southwest sites, symbiont functional responses f_s were estimated at 0.57 and 0.54, respectively, at 0.5 for Lobes A and B, and at 0.64 for Lobe C.

The estimated host functional responses for the different data sets were close to a constant, with $f_h = 0.176 \pm 0.002$ (mean $\pm$ standard deviation). As f_h values were predicted similar by the model, a sensitivity analysis was carried out on nine parameters used in the f_h estimation procedure to assess their impact on the value of f_h (Supplementary Fig. 3). The range of values tested of parameters were chosen according to existing range of species parameters from the DEB Add-my-Pet database, except for the new parameter v_{Ks}. Seven out of the nine parameters did not affect f_h value (Supplementary Fig. 3); only two parameters did, $\dot{p}_{Xmh}$ and v_{Ks}. $\dot{p}_{Xmh}$ is the maximum host specific feeding power ($J\,m^{-3}$) and v_{Ks} (-) is the food density where ingestion is half of its maximum (half-saturation coefficient). Therefore new parameter v_{Ks} was fixed to 0.005 (Supplementary Table 1) as

its value was pulled down by the model during the estimation procedure and as a low v_{Ks} value close to zero gave a f_h value close to f_h value obtained for other tested parameters in the sensitivity analysis (Supplementary Fig. 3). For the host to reach its maximum observed shell length (L_i, Supplementary Table 2), the host functional response value must be set to 0.18 rather than the conventional value of 0.8 (i.e., a high functional response value observed in the field) for consistency with the previous finding.

Symbiont dynamics with the farming model

Modeled host shell length L_h, symbiont structure V_s and reserve E_s, and host and symbiont biomasses increased with time (Figs. 1a, b, c, d and e, respectively). The symbiont state variables were computed with a fast dynamics simplification, assuming they go instantaneously to equilibrium. When the symbiont functional response f_s was low, the symbiont structure (V_s) and biomass were predicted to be high while the reserve energy (E_s) was not impacted (Figs. 1b, c and e). Hence, the symbiont reserve density ($[E_s]$) decreased with a lower f_s ($[E_s] = E_s/V_s$) (Fig. 1f). $[E_s]$ remained constant for a same f_s (Fig. 1f). The predicted symbiont structure increased dramatically when symbiont functional response was too low ($f_s < 0.5$) and reached unreasonable sizes for symbionts, becoming too large compared to observed gill sizes from the field. This indicated that the simplification of fast dynamics was no longer valid for such low values of functional responses. At the Regab Center site, the host to symbiont ratio of biomass was 8.40, predicted at 8.345 with the farming model for a symbiont functional response of 0.5653 (Supplementary Table 2). At 5 years after metamorphosis, for f_s of 1 and 0.5, symbiont dry biomass was predicted at 0.1 g and 0.2 g, respectively (Fig. 1d), and host dry biomass was estimated at 2 g for both symbiont food levels (Fig. 1b). This result falls into the range of values given by the farming model, with a final ratio of biomass Host/Symbiont of 10 for $f_s = 0.5$ and 20 for a $f_s = 1$.

Energy fluxes with the farming model

In both, the farming and the classical models, a fraction of the ingested energy by the clam host was used to increase its biomass (structure plus reserve plus reproduction buffer), another fraction was spent to cover somatic and maturity maintenance costs, yet another fraction was lost because processes are thermodynamically consistent and have intrinsic losses (assimilation, growth and reproduction overheads). Symbionts had similar use for energy, with the difference that they did not use energy for maturation or reproduction processes.

The classical model predicted a higher clam ingestion for larger specimen shell size and for higher functional responses (f) (Supplementary Fig. 4). With the farming model, the predicted symbiont and host ingestions were both higher with larger hosts, as with the classical model. However the symbiont and host ingestions remained more or less constant for different values of symbiont functional responses (f_s) (Fig. 2a, b). Comparing the ingestion values of the host in the classical model for f = 1 and a maximum host size, the clam ingestion value was 1000 $J\,d^{-1}$ compared to 2500 $J\,d^{-1}$ for symbionts and 80 $J\,d^{-1}$ for the host with the farming model (Fig. 2a, b; Supplementary Fig. 4).

Using the farming model, the variation in biomass and dissipated energy as maintenance and overheads were compared between an adult host and its symbionts for two symbiont functional responses ($f_s = 1$ and $f_s = 0.5$) and two sizes of adult clam hosts (0.8 times the maximum estimated shell length (= 10.5 cm) and 0.5 times the maximal estimated shell length (= 6.6 cm)) (Fig. 3). The variation in time of symbiont biomass (i.e., variation in the symbionts' reserve plus variation in the symbionts' structure) could not be computed with the farming model, since a fast dynamic of symbionts was assumed. Symbiont state variables were immediately adjusted to equilibrium when conditions changed such as a modification in symbiont functional response. For a different symbiont functional response (f_s), the host did not change the proportion of energy partitioned between biomass and dissipation (Figs. 3a, c, d, f, g and i). The energy dissipated by the symbionts was negligible compared to that of the host (Figs. 3a, b and c). A small host (Fig. 3b) allocated a higher fraction of its energy budget to increase its biomass compared to a larger host (Figs. 3a and c). The fraction of energy used for the reproduction buffer was substantially higher for a largest host (Fig. 3d,e) compared to smallest host size, while the smallest host used a larger fraction of energy to increase its reserve and structure (i.e., growth) (Fig. 3e). The larger the host was, the higher the percentage of mobilized energy for somatic maintenance (Figs. 3g and h). Only a small proportion of energy was lost in reproduction overheads and maturity maintenance (Figs. 3g, h and i). A low functional response did not increase the proportion of energy used for maintenance for a same host size (Figs. 3g and i).

The size of the host did not impact the way symbionts allocated their energy (Figs. 3j and k): 3/4 of the symbionts dissipated energy as growth overhead, 1/4 as assimilation overhead and a small amount for somatic maintenance. Compared to the classical model, the increase in biomass due to the reproduction buffer was significantly higher in the farming model (classical model Supplementary Fig. 5). For a same host size, a lower f_s increased symbiont energy proportion allocated to somatic maintenance (Figs. 3j and l).

Chemical element fluxes with the farming model

The farming model allowed analyzing the fluxes of carbon, oxygen and nitrogen of the host and its symbionts separately (for chemical fluxes predicted with the classical model see available information on Supplementary Fig. 6).

The host carbon, oxygen and nitrogen fluxes for assimilation (J_C^{Ah}, J_O^{Ah}, J_N^{Ah}, Figs. 4a, b, c, respectively) and for dissipation (J_C^{Dh}, J_O^{Dh}, J_N^{Dh}, Figs. 4d, e, f, respectively) increased in tandem with the host size (i.e., shell length). As expected, for smaller clam, host chemical elements used for growth increased with host size and then decreased for larger clams. This pattern was consistent with a first acceleration phase of growth and then a slowing of growth when the host approached its maximum size. Most of the assimilated chemical elements by the host (carbon, oxygen and nitrogen, Figs. 4a, b, c, respectively) were lost for dissipation processes (order of magnitude 10^{-4} mol d^{-1}) (carbon, oxygen and nitrogen, Figs. 4d, e, f, respectively) and a smaller fraction (order of magnitude 10^{-7} mol d^{-1}) was mobilized for growth (carbon, oxygen and nitrogen, Figs. 4g, h, i, respectively). Host fluxes of carbon, oxygen and nitrogen for assimilation, dissipation and growth processes were independent of symbiont functional response (f_s) (Fig. 4).

Symbionts assimilated carbon, oxygen and nitrogen (Figs. 5a, b and c, respectively) and carbon, oxygen and nitrogen used for symbionts growth (Figs. 5g, h and i, respectively) increased in tandem with host size and were constant for a given host size, independently of symbiont functional response (f_s). Dissipated carbon, oxygen and nitrogen (Figs. 5d, e and f respectively) also increased in tandem with the increase of host size, but decreased with a higher symbiont functional response (f_s). Unlike the host, symbionts used more chemicals for growth (Figs. 5g, h and i) than the amount they dissipated (Figs. 5d, e and f).

At Regab Center site, the farming model estimated a symbiont food level of 0.57 for a total oxygen consumption (i.e., host + symbionts) of 0.0012 mol d^{-1} (Supplementary Table 2). Regarding separate oxygen consumption of host and symbiont using the farming model, host total oxygen consumption was estimated at about 6.51×10^{-5} mol d^{-1} (assimilation 1.5×10^{-5} mol d^{-1} + dissipation 0.5×10^{-4} mol d^{-1} + growth 0.9×10^{-7} mol d^{-1}; Figs. 4b, e and h for host oxygen assimilation, dissipation and growth respectively) whereas total symbiont oxygen consumption was estimated about 1.93×10^{-3} mol d^{-1} (assimilation 1.2×10^{-4} mol d^{-1} + dissipation $1.2 \times 10^{e-5}$ mol d^{-1} + growth 1.8×10^{-3} mol d^{-1}; Figs. 5b, e and h for symbiont oxygen assimilation, dissipation and growth respectively). The farming model predicted that 99% of the total oxygen consumed was from the symbionts. The symbiont sulfur assimilation increased with host size but did not depend on the symbiont functional response (f_s) (Fig. 5j).

Discussion

Symbiotic associations rely on some kind of equilibrium between costs and benefits for the host and its symbionts. Symbionts can limit the fitness of the host but also can act as a buffer to stressors[41]. Symbionts can shift from beneficial to costly to the host because of external stressors making symbiotic association quite vulnerable[41]. The farming model novelty was to include within a DEB framework the bacterial sulfur-oxidizing symbionts as a dynamic system which depends on external food source (hydrogen sulfide) and temperature, and on the host clam farming feeding strategy described in the literature for deep-sea species[29]. The idea was that the host vesicomyid clam might be impacted by its symbiont dynamic as symbionts are its only food source at the adult stage. The farming model, unlike the classical model, is able to give insight into host-symbiont dynamics.

Usually, the ingestion of an organism varies proportionally to food availability and with environmental variations, as it is the case in DEB theory[36]. In the farming model, host functional response f_h was surprisingly estimated at a low and constant value. A low and constant f_h resulted in a low and stable host ingestion ($\dot{p}_{Xh}$). While f_h was constant accross sites, estimated symbiont functional responses (f_s) varied between sampling sites. This suggests that the clam ensures itself a constant functional response (f_h) that is independent of its sulfur-oxidizing symbiont functional response (f_s). Noteworthy is that both symbiont structure and symbiont biomass were larger for a lower symbiont functional response, and therefore a lower symbiont food density. When less substrate was available for the symbionts (i.e., low sulfide availability), the amount of bacterial symbionts increased so that their total ingestion of substrate remained stable and thus providing for the host constant ingestion. The symbiont has to provide food for itself, for its growth while being digested, providing also food for the host. This suggests that the amount of bacterial symbiont harbored by the host varies with its environment. Symbionts might act as a buffer to environmental food availability while host maintains a low but stable ingestion. This kind of homeostasis might be a survival strategy and a great adaptation to prosper in a fluctuating environment such as cold seeps, where the flow of sulfide can decrease for some time. This homeostasis is a novel concept compared to what has been suggested so far in the literature regarding deep-sea symbiotic species, where often the increase of symbionts within the gills of bivalves was linked to the increase level of reduced compounds such as sulfide. In *Bathymodiolus azoricus* deep-sea symbiotic mytilids, a pulse of sulfide induced an increase in sulfur-oxidizing bacteria densities[42]. The host might control its symbiont density. Symbionts have a reduced genome, where, for example, certain genes needed for bacterial division are absent or controlled by the host[9].

Bacterial symbionts are contained inside gill bacteriocytes where digestion occurs[25]. Estimated symbiont size cannot be physically above gill size. The fact that symbiont size was estimated above gill size when symbiont functional response was too

low (f_s<0.5) was interpreted as a state not consistent with a viable state of the host and was treated as a death condition for the host. Also, the fast symbiont dynamic assumption of the farming model is only valid if the symbiont can really have a fast dynamic. For lower values of f_s there may not be enough food available in the environment for the symbiont to rapidely adjust to the equilibrium given by the model's assumption. This means that only above a certain level of food this assumption can be seen as reasonable.

Adding the symbiont in the novel farming DEB model increased the complexity of *C.regab* classical DEB model by adding two state variables that define the symbiont (symbiont structure V_s and reserve E_s). Resolving the symbiont state variable equations at the same time scale of the host leads to more than a solution and increases the dimensionality and complexity of the model. Division of bacteria is quite fast in general and we assumed that symbiont dynamics were quicker than host. This time-scale separation was assumed in the construction of the farming model to enable mathematical resolution of the equations governing the symbiont state variables. Time scale separation as a mathematical solution has been applied, for example, in root-shoot and coral-symbodinium symbiose dynamic energy budget models to reduce their dimensionality, thereby simplifying these complex models[43]. At this time, only one symbiotic bacteria from a shipworm bivalve was successfully cultured[44]. However, there was no indication on time of their development. According to the review of[45], this is the only case reported for thiotrophic endosymbiont cultured. We considered symbiont fast dynamic compared to its host as a reasonable assumption given the actual knowledge on both.

The recent DEB model developed on the Atlantic deep-sea mussel *B. azoricus*[46] included its symbionts as feeding fluxes: a particulate organic matter flux from filter-feeding, a methane flux and an hydrogen sulfide flux from its endosymbionts. The methane and sulfide were considered as assimilated directly by the host, bypassing the symbionts, and were considered proportional to the surface area of the mussel gills. In this paper, symbiont assimilated fluxes from available sulfide were proportional to the symbiont volume, as they are bacteria[36]. *B. azoricus* model was simplified and focused on the bivalve growth, and did not include energy invested into maturity/reproduction of the host as do *C. regab* DEB models in this paper. Two DEB models have been developed to describe symbiotic relationships between endosymbiotic photosynthetic *Symbiodinium* algae with cnidarian, a shallow coral species[39,47] and an anemone[40]. Symbiotic anemones and corals (Cnidarians) can obtain nutrients from their environment and from their symbionts. In both symbiotic anemone and coral models, translocation of carbon from symbionts to the host was modeled as a surplus flux, with symbionts using first the fixed photosynthetically carbon they needed while the remaining became available for the host. In both model, priority access to nitrogen was given to the host; however, symbiont access was modeled differently between the two models. In the anemone - *Symbiodinium* model, symbionts received nitrogen from host surplus flux while in the coral - *Symbiodinium*, they received nitrogen by "consuming" the host, as in a predator-prey relationship. Such translocation fluxes of nutrients from host to symbionts were not implemented in the *C. regab* farming model although they could occur. These exchanges of nutrients remain poorly understood in deep-sea chemosymbiotic bivalves. In the farming model, symbionts access to carbon and nitrogen first, and then the host can obtain carbon and nitrogen by feeding on the symbionts. Countless symbiotic states happen in life[48], and these three models show different degrees of food dependency and equilibrium between host and symbionts. The C. regab farming model with explicit symbionts is complex. The model could be simplified, as in anemone - *Symbiodinium* (2 state variables, symbionts and host biomasses)[40] and coral - *Symbiodinium* (3 state variables, symbionts and host biomasses and photooxidative synthesizing unit)[47] models to answer specific scientific questions (i.e., symbiont cost and coral response photooxidative stress, respectively) and to prevent excessive model complexity. As there were fewer state variables (no reserve, no maturity, and no reproduction buffer) in these models, the number of parameters was reduced. The first published coral - *Symbiodinium* model[39] was much more complex than the second one[47] which focused on the question of coral response to photooxidative stress. Complexifying the farming model to add additional reserves (e.g., stored sulfur granules by sulfur-oxidizing symbionts) and/or adding additional food sources for the host and its symbionts (e.g., nutrient translocation) might require some model simplification to keep the model usable[43].

Despite the use of DEB standard compositions for structure and reserve, both classical and farming model predicted well elemental fluxes. A noteworthy result was that modeled symbiont and host dioxygen fluxes with farming model support the idea that most of oxygen consumed by the whole symbiotic association is by the symbionts. In some symbioses, the oxygen consumption rates may be so high that oxygen could be a limiting factor for the host and symbiont metabolisms[33]. The high oxygen demand of chemosynthetic symbionts places a cost on their hosts that have evolved a range of adaptations to meet the aerobic demands of their symbionts[33].

The mean sulfide consumption by symbionts in *C. regab* gills used in this study to calibrate the farming model was much lower than that in the vesicomyid species *Calyptogena kilmeri* and *C. pacifica* from cold seep sites in Monterey Bay, U.S. state of California[49]. The mean gill consumption values were 0.13 and 0.96 µmol gill Ww g^{-1} min^{-1} for *C. kilmeri* and *C. pacifica*, respectively, while the *C. regab* gill consumption were 0.021, 0.036 and 0.052 µmol gill Ww g^{-1} min^{-1} for the Regab Center, Regab Southwest and Lobe C sites, respectively. However, the farming model predicted a consumption of sulfide around 2-fold higher for *C. regab* than the on-site measured values used to calibrate the model, getting closer to the values measured *in situ* in Monterey Bay on the other vesicomyid species.

C. regab sulfur-oxidizing symbiont yields of sulfate and oxygen for hydrogen sulfide assimilation were predicted similar to those of *Thiobacillus denitrificans* yields[50]. On the contrary, the yield of moles of ammonium for sulfide assimilation was predicted to be much higher than the one of *Thiobacillus denitrificans*. The yield was predicted by the model to be 1.8 mol NH_4^+ per mol of H_2S (NH_4^+/H_2S) instead of 0.1 mol NH_4^+/H_2S (RE = 17.08). This yield of 0.1 NH_4^+/H_2S, as well as other symbionts yields implemented in the farming model (SO_4^{2-}/H_2S, O_2/H_2S, biomass/H_2S, HS^-/biomass), were used as indicators to help calibrating the model. Those calibrating yields were obtained from batch cultures of the sulfur-oxidizing bacteria *Thiobacillus denitrificans*[50]. At this time, it was not yet possible to cultivate symbionts from deep-sea symbiotic species in order to determine the stoichiometry of hydrogen sulfide oxidation by deep-sea sulfur-oxidizing bacteria. Only recently symbiotic strains from a symbiotic shipworm bivalve was successfully cultured[44]. What the critical error meant on nitrogen yield prediction in our study, was that this yield of 0.1 mol of NH_4^+/H_2S (which was for *Thiobacillus denitrificans*) did not fit well the actual data of the symbionts of *C. regab*, and that a yield of 1.8 was a better fit for the macrochemical equations of our study, solved by the farming model.

The hypothesis of an important energy fraction allocated to maintenance, as observed in our results, was made in a static bioenergetic model developed for the vesicomyid species *C. kilmeri* and *C. magnifica* from cold seeps, up to 30–50% of the total energy budget[51]. Symbiont sulfide oxidation produces proton and sulfate ions which could result in acidic conditions if they accumulate. To maintain ion homeostasis, the authors hypothesized that the clams needed energy to eliminate protons[51]. The results of this latter paper suggested that the fraction of energy allocated to maintenance could be near 75% of the total energy budget for the largest specimens.

In this study, the classical and the farming models provided good results as small errors were calculated (MRE, SMAE, SMSE) for predictions from the estimated set of parameters and data, collected from the field and laboratory experiments. The farming model is more complex than the classical model, since it has more state-variables, fluxes, and ten more parameters, but it allows for extra predictions that are bound to increase the error. More than half of the data (8 out of the 13 different data used in both models) were better predicted with the farming model (e.g., growth rate of the host) than with the classical model. In addition, parameters related to the symbiont bioenergetics could be deciphered with this novel farming model, highlighting the importance of integrating symbionts within the dynamic of the energy budget of a symbiotic model species to study host-symbiont relationship.

For the classical model there was a need to use an anchor data point for the growth rate to have the estimation, set at 1 cm yr^{-1}. Without this anchor data point, the classical model growth was predicted too fast compared to the literature values. A growth rate was estimated at 0.8 cm yr^{-1} for both Regab center and south-west sites using a cohort analysis on adult specimens[25]. The anchor data point for the growth rate was not needed for the farming model to obtain realistic growth rate values. Both classical and farming models presented in this paper predicted growth rates for small *Christineconcha regab* specimens at Regab sites southwest and center of the same order of magnitude as the vesicomyid *Calyptogena kilmeri*[52]. The growth rate of *C. kilmeri* from a cold seep off central California was estimated by *in situ* experiment at 1 to 2 cm yr^{-1} for small specimens[52]. With radionuclide dating techniques on shells, the vesicomyid species growth rate from the Galápagos Spreading Center hydrothermal field and 21°N East Pacific Rise hydrothermal area was estimated at 4 cm yr^{-1}[53] and an average growth rate along the axis of maximum growth (10 cm) of 0.27 cm yr^{-1}[54], respectively.

Modeled functional responses were directly linked to food density. Comparing all sites, the functional response was estimated to be the highest at the Lobe C site by both the farming (for symbionts) and classical models (whole symbiotic association). With the farming model, the functional response (for symbionts) was estimated the lowest at Lobe A and B sites while with the classical model, the lowest estimated functional response was at the southwest and center sites of the Regab pockmark.

Among the three Lobe sites, the Lobe C site biogeochemical context seemed to provide the best conditions for sulfide production and thus a higher functional response for *C. regab* symbionts, which is consistent with the Lobe C site having the highest estimated functional response. In the Lobes, cold seep-like ecosystems are formed thanks to important deposits of organic material coming from the Congo River. At Lobe C, sedimentation rates were high compared to Lobes A and B, and dense and alive vesicomyid aggregates were dominated by *C. regab* with few dead shells only[55,56]. Additionally, it was supposed that this site was the most recent deposition zone[55,56]. At Lobe A, vesicomyids also formed dense beds dominated by *C. regab*. The Lobe B site had only small patches of reduced sediments, and few scattered vesicomyid patches mainly consisting of dead shells; moreover, *C. regab* was not the main vesicomyid species[56].

With both classical and farming models, the functional response was estimated higher for the center of Regab pockmark than for the southwestern site, which agrees with what was observed in the field. At the Regab site, a gradient of methane emission occurs along the pockmark radius from the center to the periphery[57]. The highest sulfur content was measured in the sediment located in the center of the pockmark[17]. Furthermore, a higher biomass and condition index on site was measured for specimens collected from the center than from the southwestern site[25].

Predictions of *C. regab* symbiont sulfur consumption rates were estimated higher for the Regab southwest and center

specimens than for the Lobe C specimens. The farming model suggested that a higher symbiont consumption was linked to a lower symbiont functional response. Experimental data showed that the *C. regab* sulfur consumption rate of the gills from *C. regab* was higher for Regab's southwestern site, then Lobe C, and finally the Regab center. One explanation of these differences could be that for the sulfide experiment, the same functional response was set to be estimated for the specimens at the three different sites, as during the experiment, they were exposed to the same food density, since they were likely not in the field. Symbiont functional responses are complex to explain, as symbionts' access to sulfide may be related not only to the concentration of sulfide in the near environment but also to how much/and how the host provides sulfide to its symbionts (host sulfide binding capacity and foraging capacity) and to sulfur storage by symbionts as granules and circulating sulfide inside the host[7]. The total elemental sulfur of *C. regab* specimens was analyzed, and a difference between Lobe C site specimens and Regab center site specimens was observed, with a mean percentage of elemental sulfur of 12.7% at the Lobe C site compared 16% at the Regab center site[20]. Elemental sulfur granules were also found in other vesicomyid species gills, produced by sulfur-oxidizing symbionts and could constitute a "reserve" to buffer environmental fluctuations in sulfide availability[7]. Adding an additional reserve for sulfur would be interesting to try to understand the dynamics of those granules, their formation and their use by the sulfur-oxidizing symbionts.

Methods

Model description

The classical model

DEB theory has been widely applied to bivalve species (> 140 species). The classical DEB model used is this paper is the abj model (abj: metabolic acceleration (a) between "birth" (b) and "metamorphosis" (j)) which is the most applied to bivalves[58]. The abj model includes four state variables: reserve E (J), structure V (cm^3), maturity level E_H (J) and reproduction buffer E_R (J) (Fig. 6a, Table 1). This abj model has four life stages: embryo, juvenile I, juvenile II and adult with three transitions between life stages (birth E_H^b, metamorphosis E_H^j and puberty E_H^p) which occur when that level of maturity E_H is reached (Fig. 7). During the embryo stage, the organism does not feed and relies on its egg reserves. After birth, the juvenile organism can feed on external food sources but cannot reproduce yet. When puberty E_H^p is reached, the organism no longer needs to allocate energy to increase its maturity and instead starts allocating energy to the reproduction buffer (Fig. 7)[36,59].

The main difference from the standard DEB model is the existence of metamorphosis. For bivalves, metamorphosis corresponds to a metabolic switch resulting in the transition from planktonic to benthic life with morphological changes (loss of the velum of the umbo-veliger larva and development of the foot of the pediveliger larva) (Fig. 7). Metabolically, during the juvenile I phase, an acceleration occurs until it reaches metamorphosis. This acceleration is modeled by the increase of food assimilation into reserve $\dot{p}_A$ and energy reserve mobilization $\dot{p}_C$. Two parameters, the maximum specific assimilation rate $\{\dot{p}_{Am}\}$ and the energy conductance $\dot{v}$, increase in tandem to model these effects (See assimilation and mobilization fluxes formulae Table 1 and acceleration coefficient Table 2). This leads to an exponential growth for juvenile I. In subsequent life stages, the growth follows von Bertalanffy curve for constant food availability.

The classical model parameters were listed in Table 3.

The farming model

The novel farming model was built from the *Christineconcha regab* abj model by considering that the symbiont has a different dynamic than the host. This model was based on the "farming" feeding strategy of the host and named farming to distinguish from the classical abj model. The model was built by integrating the sulfur-oxidizing bacteria into an abj model of the clam host (Figs. 6b and c). Symbionts macrochemical equations for assimilation, dissipation and growth transformations were explicitly taken into account using a standard composition for reserve and structure $CH_{1.8}O_{0.5}N_{0.15}$[36] (Supplementary Methods 1.5). As bacteria divide, they do not need to invest energy into a reproduction buffer as the clam host does. Therefore, the state variables were reduced to only two: reserve E_s and structure V_s (Table 4). Also, the bacterial symbionts were modeled with a single juvenile stage (Fig. 7). The symbiont population is modeled with the same dynamics as a single bacterium. Unicellular organisms that divide into two daughter cells are well modeled as V1-morphs (changing its shape as it grows)[36]. Symbiont population has an ingestion rate proportional to its structure V ($\dot{p}_{Xs}$, Table 4)[36]. Symbiont fluxes describing ingestion, assimilation, mobilization, maintenance and growth were added (Fig. 6b, Table 4). The clam ingestion flux came from the symbiont reserve and structure they harbor in their gills (Figs. 6b and c, Table 4). This model has ten extra parameters related to the symbionts (Table 4).

Biological data for model parameterization

Several cruises were undertaken to explore the Congo submarine channel and cold seep ecosystems in the Gulf of Guinea (South–East Atlantic, Supplementary Fig. 7). Samples and experimental data acquired during these different cruises provided the data used to parameterize the models (Supplementary Table 4). Specimens came from two major areas: the end of the Congo submarine channel named the Lobe complex (Lobes A, B and C), and the Regab pockmark (Center and Southwest)[20].

Forcing variables for parameter estimation: functional response and temperature

In the classical abj model, the functional response (f) follows the Michaelis–Menten function (Eq. 1). X is the food density, X_K is the half saturation coefficient and x is the scaled food density[36].

$$f = \frac{\frac{X}{X_K}}{1+\frac{X}{X_K}} = \frac{x}{1+x} \tag{1}$$

In the *C. regab* classical model, a functional response was estimated as a parameter for each sampling site, regardless of the time/season of sampling: Regab Center, Regab Southwest, Lobe A, Lobe B and Lobe C (Supplementary Table 3). Regarding the Regab pockmark, it has been suggested that biogeochemical conditions have been relatively stable throughout time, at least between 2000 and 2008[57]. However, the Lobes complex was characterized by high sediment accumulation and turbidity currents and appeared to be a less stable environment than Regab[60,61]. Nevertheless, for the parameter estimations, food (i.e., sulfide) was assumed to be more or less constant at each Lobe and Regab site throughout the years of sampling.

In the farming model, a functional response for symbionts (f_s) was defined in the same fashion as the functionnal response f in the classical model; one f_s was set to be estimated as a parameter for each sampling site. The novelty was that the quantity of food available for the host was considered dependent on the ratio between symbiont structure (V_s) and host structure (V); this will take into account that for the same volume of symbionts, a larger host will have a lower functional response. A new parameter was added, the half saturation coefficient v_{Ks}, where host ingestion is half of its maximum (Eq. 2).

$$f_h = \frac{\frac{V_s}{V}}{\frac{V_s}{V}+v_{Ks}} \tag{2}$$

Host functional responses (f_h) were computed assuming the dynamics of the symbiont was very fast compared to the dynamics of the host, and that the available foods for the host were the structure and reserve of the symbiont (Supplementary Methods 1.9). The connection of the functional response with the ingested flux of the host is given by Eq. 3. $\dot{p}_X$ is the host ingestion flux ($J\,d^{-1}$), $\{\dot{p}_{Xm}\}$ is the maximum host ingestion flux ($J\,d^{-1}\,cm^{-2}$), s_M (-) is the host acceleration factor, V (cm^3) is the host structure.

$$f_h = \frac{\dot{p}_X}{\{\dot{p}_{Xm}\}\,s_M V^{2/3}} \tag{3}$$

According to the above equations (Eq. 2 and 3), host functional responses (f_h) were estimated by the farming model for each data set using corresponding host structural lengths (L_h) and model's parameters (Supplementary Methods 1.1, predict_Christineconcha_regab.m file).

The impact of temperature was dealt with the standard temperature correction using the Arrhenius temperature (Supplementary Methods A.6)[36].

Estimation of primary parameters

The Add-my-Pet (AmP) procedure (DEB-tool package, Matlab)[59,62] was used to estimate *C. regab* farming and classical parameters (Supplementary Table 1) from data (Supplementary Table 4) at a given temperature and functional responses. Parameters were obtained using a minimization method of a loss function (function of data, predictions from parameters and data weight coefficients)[63]. The accuracy of the models fit was quantified with the mean relative error (MRE), the symmetric mean squared error (SMSE) and the standardized mean absolute error (SMAE). Constraints were added as customized filters for the symbionts to keep the estimation of parameters inside the biologically meaningful part of the parameter space during the minimization procedure. Additional codes for predictions (Supplementary Methods 1.7, 1.8 and 1.9), compared to those available on the Add-My-Pet database, were developed in this study for new data types in the farming model (Supplementary Methods 1).

Data availability

The datasets generated and/or analysed during the current study are available in the Christineconcha_regab_dynamic_energy_budget repository, https://github.com/mvdb26/Christineconcha_regab_dynamic_energy_budget.

References

1. Dubilier, N., Bergin, C. & Lott, C. Symbiotic diversity in marine animals: the art of harnessing chemosynthesis. *Nat. reviews. Microbiol.* **6**, 725–740, DOI: 10.1038/nrmicro1992 (2008).

2. Krylova, E. M. & Sahling, H. Vesicomyidae (Bivalvia): current taxonomy and distribution. *PLOS ONE* **5**, e9957, DOI: 10.1371/journal.pone.0009957 (2010).

3. Johnson, S. B., Krylova, E. M., Audzijonyte, A., Sahling, H. & Vrijenhoek, R. C. Phylogeny and origins of chemosynthetic vesicomyid clams. *Syst. Biodivers.* **15**, 346–360, DOI: 10.1080/14772000.2016.1252438 (2017).

4. Decker, C., Olu, K., Arnaud-Haond, S. & Duperron, S. Physical proximity may promote lateral acquisition of bacterial symbionts in vesicomyid clams. *PLOS ONE* **8**, e64830, DOI: 10.1371/journal.pone.0064830 (2013).

5. Newton, I. L. G., Girguis, P. R. & Cavanaugh, C. M. Comparative genomics of vesicomyid clam (Bivalvia: Mollusca) chemosynthetic symbionts. *BMC Genomics* **9**, 585, DOI: 10.1186/1471-2164-9-585 (2008).

6. Stewart, F. J. & Cavanaugh, C. M. Pyrosequencing analysis of endosymbiont population structure: co-occurrence of divergent symbiont lineages in a single vesicomyid host clam. *Environ. Microbiol.* **11**, 2136–2147, DOI: 10.1111/j.1462-2920.2009.01933.x (2009).

7. Cruaud, P. *et al.* Ecophysiological differences between vesicomyid species and metabolic capabilities of their symbionts influence distribution patterns of the deep-sea clams. *Mar. Ecol.* **40**, e12541, DOI: 10.1111/maec.12541 (2019).

8. Ip, J. C.-H. *et al.* Host–endosymbiont genome integration in a deep-sea chemosymbiotic clam. *Mol. Biol. Evol.* **38**, 502–518, DOI: 10.1093/molbev/msaa241 (2021).

9. Perez, M. *et al.* Divergent paths in the evolutionary history of maternally transmitted clam symbionts. *Proc. Royal Soc. B: Biol. Sci.* **289**, 20212137, DOI: 10.1098/rspb.2021.2137 (2022).

10. Szafranski, K. M., Gaudron, S. M. & Duperron, S. Direct evidence for maternal inheritance of bacterial symbionts in small deep-sea clams (Bivalvia: Vesicomyidae). *Naturwissenschaften* **101**, 373–383, DOI: 10.1007/s00114-014-1165-3 (2014).

11. Ikuta, T. *et al.* Surfing the vegetal pole in a small population: extracellular vertical transmission of an 'intracellular' deep-sea clam symbiont. *Royal Soc. Open Sci.* **3**, 160130, DOI: 10.1098/rsos.160130 (2016).

12. Cary, S. C. & Giovannoni, S. J. Transovarial inheritance of endosymbiotic bacteria in clams inhabiting deep-sea hydrothermal vents and cold seeps. *Proc. Natl. Acad. Sci.* **90**, 5695–5699, DOI: 10.1073/pnas.90.12.5695 (1993).

13. Stewart, F. J., Young, C. R. & Cavanaugh, C. M. Lateral symbiont acquisition in a maternally transmitted chemosynthetic clam endosymbiosis. *Mol. Biol. Evol.* **25**, 673–687, DOI: 10.1093/molbev/msn010 (2008).

14. Ozawa, G. *et al.* Ancient occasional host switching of maternally transmitted bacterial symbionts of chemosynthetic vesicomyid clams. *Genome Biol. Evol.* **9**, 2226–2236, DOI: 10.1093/gbe/evx166 (2017).

15. Peek, A. S., Feldman, R. A., Lutz, R. A. & Vrijenhoek, R. C. Cospeciation of chemoautotrophic bacteria and deep sea clams. *Proc. Natl. Acad. Sci.* **95**, 9962–9966, DOI: 10.1073/pnas.95.17.9962 (1998).

16. von Cosel, R. & Olu, K. Large Vesicomyidae (Mollusca: Bivalvia) from cold seeps in the Gulf of Guinea off the coasts of Gabon, Congo and northern Angola. *Deep. Sea Res. Part II: Top. Stud. Oceanogr.* **56**, 2350–2379, DOI: 10.1016/j.dsr2.2009.04.016 (2009).

17. Ondréas, H. *et al.* ROV study of a giant pockmark on the Gabon continental margin. *Geo-Marine Lett.* **25**, 281–292, DOI: 10.1007/s00367-005-0213-6 (2005).

18. Bridges, A. *et al.* Review of the central and south atlantic shelf and deep-sea benthos: science, policy, and management. In *Oceanography and Marine Biology*, 127–218, DOI: 10.1201/9781003363873-5 (CRC Press, 2023), 1 edn.

19. Olu, K. *et al.* Influence of seep emission on the non-symbiont-bearing fauna and vagrant species at an active giant pockmark in the Gulf of Guinea (Congo–Angola margin). *Deep. Sea Res. Part II: Top. Stud. Oceanogr.* **56**, 2380–2393, DOI: 10.1016/j.dsr2.2009.04.017 (2009).

20. Khripounoff, A. *et al.* Respiration of bivalves from three different deep-sea areas: Cold seeps, hydrothermal vents and organic carbon-rich sediments. *Deep. Sea Res. Part II: Top. Stud. Oceanogr.* **142**, 233–243, DOI: 10.1016/j.dsr2.2016.05.023 (2017).

21. Rabouille, C. *et al.* Carbon and silica megasink in deep-sea sediments of the Congo terminal lobes. *Quat. Sci. Rev.* **222**, 105854, DOI: 10.1016/j.quascirev.2019.07.036 (2019).

22. Olive, G., Rodrigues, C. F. & Cunha, M. R. Chemosymbiotic bivalves from the mud volcanoes of the Gulf of Cadiz, NE Atlantic, with descriptions of new species of Solemyidae, Lucinidae and Vesicomyidae. *ZooKeys* 1–38, DOI: 10.3897/zookeys.113.1402 (2011).

23. Rodrigues, C. F., Hilário, A. & Cunha, M. R. Chemosymbiotic species from the Gulf of Cadiz (NE Atlantic): distribution, life styles and nutritional patterns. *Biogeosciences* **10**, 2569–2581, DOI: 10.5194/bg-10-2569-2013 (2013).

24. Krylova, E. M., Sahling, H. & Janssen, R. Abyssogena: a new genus of the family Vesicomyidae (Bivalvia) from deep-water vents and seeps. *J. Molluscan Stud.* **76**, 107–132, DOI: 10.1093/mollus/eyp052 (2010).

25. Decker, C. *Diversité, écologie et adaptation des bivalves Vesicomyidae associés aux environnements réducteurs profonds des marges continentales*. Ph.D. thesis, Brest (2011).

26. Boetius, A. *et al.* A marine microbial consortium apparently mediating anaerobic oxidation of methane. *Nature* **407**, 623–626, DOI: 10.1038/35036572 (2000).

27. Pruski, A. M. *et al.* Energy transfer in the Congo deep-sea fan: From terrestrially-derived organic matter to chemosynthetic food webs. *Deep. Sea Res. Part II: Top. Stud. Oceanogr.* **142**, 197–218, DOI: 10.1016/j.dsr2.2017.05.011 (2017).

28. Childress, J. J. & Girguis, P. R. The metabolic demands of endosymbiotic chemoautotrophic metabolism on host physiological capacities. *J. Exp. Biol.* **214**, 312–325, DOI: 10.1242/jeb.049023 (2011).

29. Sogin, E. M., Leisch, N. & Dubilier, N. Chemosynthetic symbioses. *Curr. Biol.* **30**, R1137–R1142, DOI: 10.1016/j.cub.2020.07.050 (2020).

30. Lan, Y. *et al.* Host–Symbiont Interactions in Deep-Sea Chemosymbiotic Vesicomyid Clams: Insights From Transcriptome Sequencing. *Front. Mar. Sci.* **6**, 680, DOI: 10.3389/fmars.2019.00680 (2019).

31. Fiala-Medioni, A. & Le Pennec, M. Trophic structural adaptations in relation to the bacterial association of bivalve molluscs from hydrothermal vents and subduction zones. *Symbiosis* 63–74 (1987).

32. Newton, I. L. G. *et al.* The *Calyptogena magnifica* chemoautotrophic symbiont genome. *Science* **315**, 998–1000, DOI: 10.1126/science.1138438 (2007).

33. Sogin, E. M., Kleiner, M., Borowski, C., Gruber-Vodicka, H. R. & Dubilier, N. Life in the dark: phylogenetic and physiological diversity of chemosynthetic symbioses. *Annu. Rev. Microbiol.* **75**, 695–718, DOI: 10.1146/annurev-micro-051021-123130 (2021).

34. Husson, B. *et al.* Modelling the interactions of the hydrothermal mussel Bathymodiolus azoricus with vent fluid. *Ecol. Model.* **377**, 35–50, DOI: 10.1016/j.ecolmodel.2018.03.007 (2018).

35. Martins, I. *et al.* Size-dependent variations on the nutritional pathway of Bathymodiolus azoricus demonstrated by a C-flux model. *Ecol. Model.* **217**, 59–71, DOI: 10.1016/j.ecolmodel.2008.05.008 (2008).

36. Kooijman, S. A. L. M. *Dynamic energy budget theory for metabolic organisation* (Cambridge University Press, 2010).

37. Gaudron, S. M., Lefebvre, S. & Marques, G. M. Inferring functional traits in a deep-sea wood-boring bivalve using dynamic energy budget theory. *Sci. Reports* **11**, 22720, DOI: 10.1038/s41598-021-02243-w (2021).

38. Martins, I. *et al.* Developing a dynamic energy budget model to project potential effects of deep-sea mining plumes on the Atlantic deep-sea mussel, *Bathymodiolus azoricus*. *Ecol. Informatics* **83**, 102803, DOI: 10.1016/j.ecoinf.2024.102803 (2024).

39. Muller, E. B., Kooijman, S. A. L. M., Edmunds, P. J., Doyle, F. J. & Nisbet, R. M. Dynamic energy budgets in syntrophic symbiotic relationships between heterotrophic hosts and photoautotrophic symbionts. *J. Theor. Biol.* **259**, 44–57, DOI: 10.1016/j.jtbi.2009.03.004 (2009).

40. Kaare-Rasmussen, J. O., Moeller, H. V. & Pfab, F. Modeling food dependent symbiosis in *Exaiptasia pallida*. *Ecol. Model.* **481**, 110325, DOI: 10.1016/j.ecolmodel.2023.110325 (2023).

41. Bénard, A., Vavre, F. & Kremer, N. Stress & symbiosis: heads or tails? *Front. Ecol. Evol.* **8** (2020).

42. Halary, S., Riou, V., Gaill, F., Boudier, T. & Duperron, S. 3D FISH for the quantification of methane- and sulphur-oxidising endosymbionts in bacteriocytes of the hydrothermal vent mussel Bathymodiolus azoricus. *ISME J.* **2(3)**, 284 (2008).

43. Pfab, F. *et al.* Timescale separation and models of symbiosis: state space reduction, multiple attractors and initialization. *Conserv. Physiol.* **10**, coac026, DOI: 10.1093/conphys/coac026 (2022).

44. Distel, D. L. *et al.* Discovery of chemoautotrophic symbiosis in the giant shipworm Kuphus polythalamia (Bivalvia: Teredinidae) extends wooden-steps theory. *Proc. Natl. Acad. Sci.* **114**, E3652–E3658, DOI: 10.1073/pnas.1620470114 (2017).

45. Petersen, J. M. & Yuen, B. The Symbiotic "All-Rounders": Partnerships between Marine Animals and Chemosynthetic Nitrogen-Fixing Bacteria. *Appl. Environ. Microbiol.* **87**, e02129–20, DOI: 10.1128/AEM.02129-20 (2021).

46. Martins, G. The metabolic theory of ecology as a mechanistic approach. In Cordovil, J. L., Santos, G. & Vecchi, D. (eds.) *New Mechanism: Explanation, Emergence and Reduction*, 29–60, DOI: 10.1007/978-3-031-46917-6_3 (Springer International Publishing, Cham, 2024).

47. Cunning, R., Muller, E. B., Gates, R. D. & Nisbet, R. M. A dynamic bioenergetic model for coral-Symbiodinium symbioses and coral bleaching as an alternate stable state. *J. Theor. Biol.* **431**, 49–62, DOI: 10.1016/j.jtbi.2017.08.003 (2017).

48. Kooijman, S. A. L. M., Auger, P., Poggiale, J. C. & Kooi, B. W. Quantitative steps in symbiogenesis and the evolution of homeostasis. *Biol. Rev.* **78**, 435–463, DOI: 10.1017/S1464793102006127 (2003).

49. Goffredi, S. K. & Barry, J. P. Species-specific variation in sulfide physiology between closely related Vesicomyid clams. *Mar. Ecol. Prog. Ser.* **225**, 227–238, DOI: 10.3354/meps225227 (2002).

50. Sublette, K. L. Aerobic oxidation of hydrogen sulfide by *Thiobacillus denitrificans*. *Biotechnol. Bioeng.* **29**, 690–695, DOI: 10.1002/bit.260290605 (1987).

51. Goffredi, S. K. & Barry, J. P. Energy acquisition and allocation in vesicomyid symbioses. *Cahiers de Biol. Mar.* **43**, 345–350, DOI: 10.21411/CBM.A.5ADE9CC5 (2002).

52. Barry, J. P., Whaling, P. J. & Kochevar, R. K. Growth, production, and mortality of the chemosynthetic vesicomyid bivalve, Calyptogena kilmeri from cold seeps off central California. *Mar. Ecol.* **28**, 169–182, DOI: 10.1111/j.1439-0485.2007.00119.x (2007).

53. Turekian, K. K. & Cochran, J. K. Growth Rate of a Vesicomyid Clam from the Galápagos Spreading Center. *Science* **214**, 909–911, DOI: 10.1126/science.214.4523.909 (1981).

54. Turekian, K. K., Cochran, J. K. & Bennett, J. T. Growth rate of a vesicomyid clam from the 21° N East Pacific Rise hydrothermal area. *Nature* **303**, 55–56, DOI: 10.1038/303055a0 (1983).

55. Olu, K. *et al.* Cold-seep-like macrofaunal communities in organic- and sulfide-rich sediments of the Congo deep-sea fan. *Deep. Sea Res. Part II: Top. Stud. Oceanogr.* **142**, 180–196, DOI: 10.1016/j.dsr2.2017.05.005 (2017).

56. Rabouille, C. *et al.* The Congolobe project, a multidisciplinary study of Congo deep-sea fan lobe complex: Overview of methods, strategies, observations and sampling. *Deep. Sea Res. Part II: Top. Stud. Oceanogr.* **142**, 7–24, DOI: 10.1016/j.dsr2.2016.05.006 (2017).

57. Pop Ristova, P. *et al.* Bacterial diversity and biogeochemistry of different chemosynthetic habitats of the REGAB cold seep (West African margin, 3160 m water depth). *Biogeosciences* **9**, 8337–8385, DOI: 10.5194/bgd-9-8337-2012 (2012).

58. Add-My-Pet Species List. https://www.bio.vu.nl/thb/deb/deblab/add_my_pet/species_list.html (2024).

59. Marques, G. M. *et al.* The AmP project: Comparing species on the basis of dynamic energy budget parameters. *PLOS Comput. Biol.* **14**, e1006100, DOI: 10.1371/journal.pcbi.1006100 (2018).

60. Rabouille, C., Baudin, F., Dennielou, B. & Olu, K. Organic carbon transfer and ecosystem functioning in the terminal lobes of the Congo deep-sea fan: outcomes of the Congolobe project. *Deep. Sea Res. Part II: Top. Stud. Oceanogr.* **142**, 1–6, DOI: 10.1016/j.dsr2.2017.07.006 (2017).

61. Sen, A. *et al.* Fauna and habitat types driven by turbidity currents in the lobe complex of the Congo deep-sea fan. *Deep. Sea Res. Part II: Top. Stud. Oceanogr.* **142**, 167–179, DOI: 10.1016/j.dsr2.2017.05.009 (2017).

62. Lika, K. *et al.* The "covariation method" for estimating the parameters of the standard Dynamic Energy Budget model I: Philosophy and approach. *J. Sea Res.* **66**, 270–277, DOI: 10.1016/j.seares.2011.07.010 (2011).

63. Marques, G. M., Lika, K., Augustine, S., Pecquerie, L. & Kooijman, S. A. L. M. Fitting multiple models to multiple data sets. *J. Sea Res.* **143**, 48–56, DOI: 10.1016/j.seares.2018.07.004 (2019).

Funding

Marine Vandenberghe was funded by a PhD fellowship provided by the CNRS through the 80-Prime Program. This work was financially supported by both the French National Program EC2CO and the 80-Prime Program.

Author contributions statement

S.M.G. conceived the project. M.V. and G.M. designed the new farming model. M.V. wrote the manuscript with inputs of S.M.G and G.M.. A.C.A., C.D., K.O. and S.D. performed some experimentations and provided data. All authors reviewed the manuscript.

Additional information

The authors declare no competing interests.

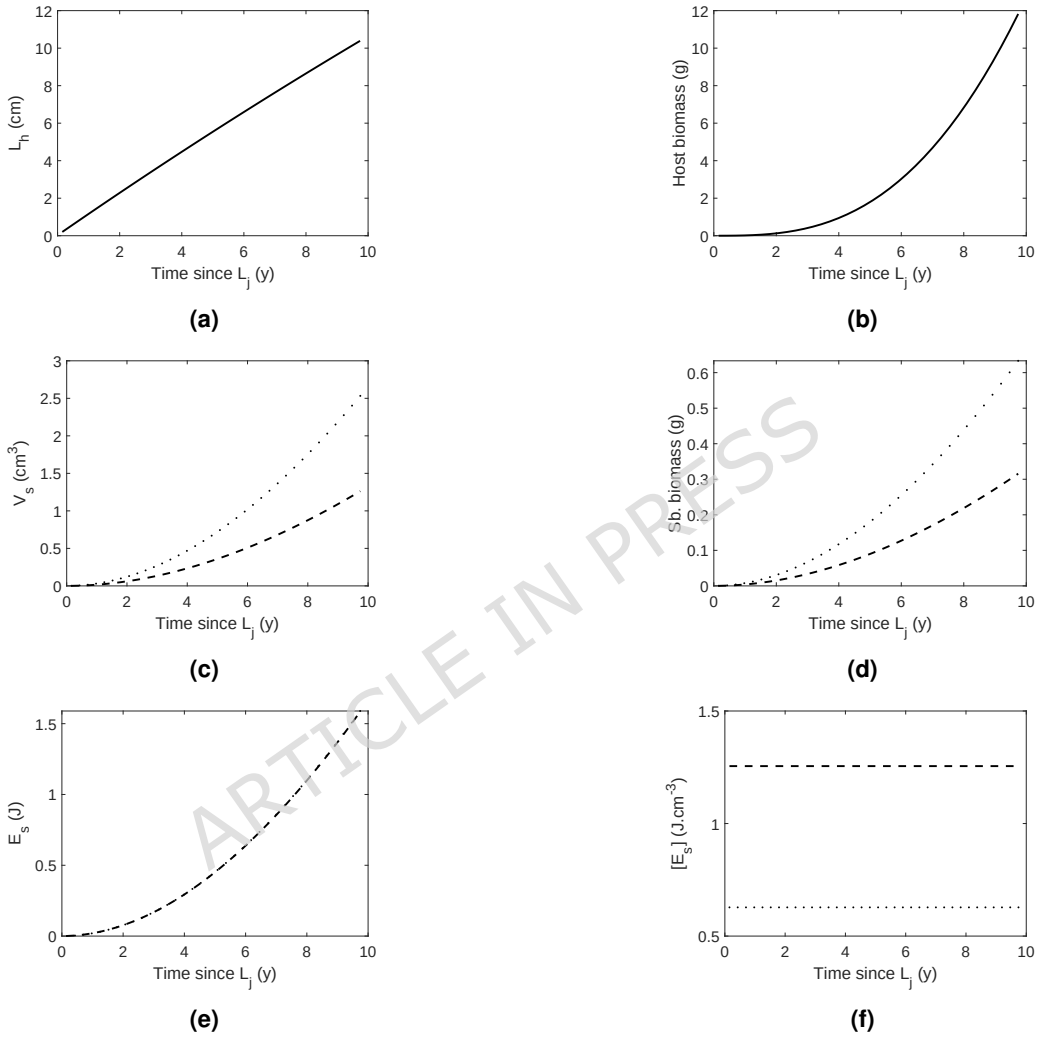

Figure 1. Modeled *Christineconcha regab* clam and its sulfur-oxidizing symbionts variables for 10 years since host clam metamorphosis (L_j = 0.1991 cm) using *C. regab* farming model (T = 2.55°C and host functional response f_h = 0.18). (c, d, e, f): dashed line (- -), symbiont functional response f_s = 1; dotted line (...), f_s = 0.5. (a) host shell length (L_h, cm); (b) host biomass (structure+reserve) (in dry weight, g); (c) symbionts structure (V_s, cm^3); (d) symbionts (Sb.) biomass (structure+reserve) (in dry weight, g); (e) symbionts reserve (E_s, J); (f) symbionts reserve density (reserve/structure) ($[E_s]$, $J\,cm^{-3}$).

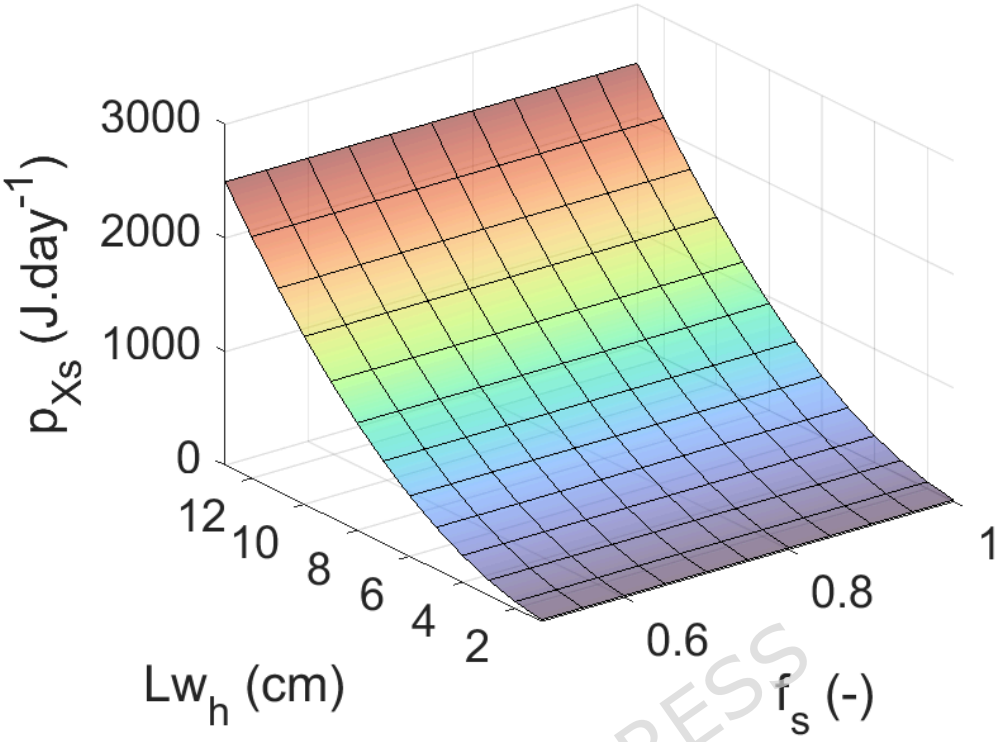

(a)

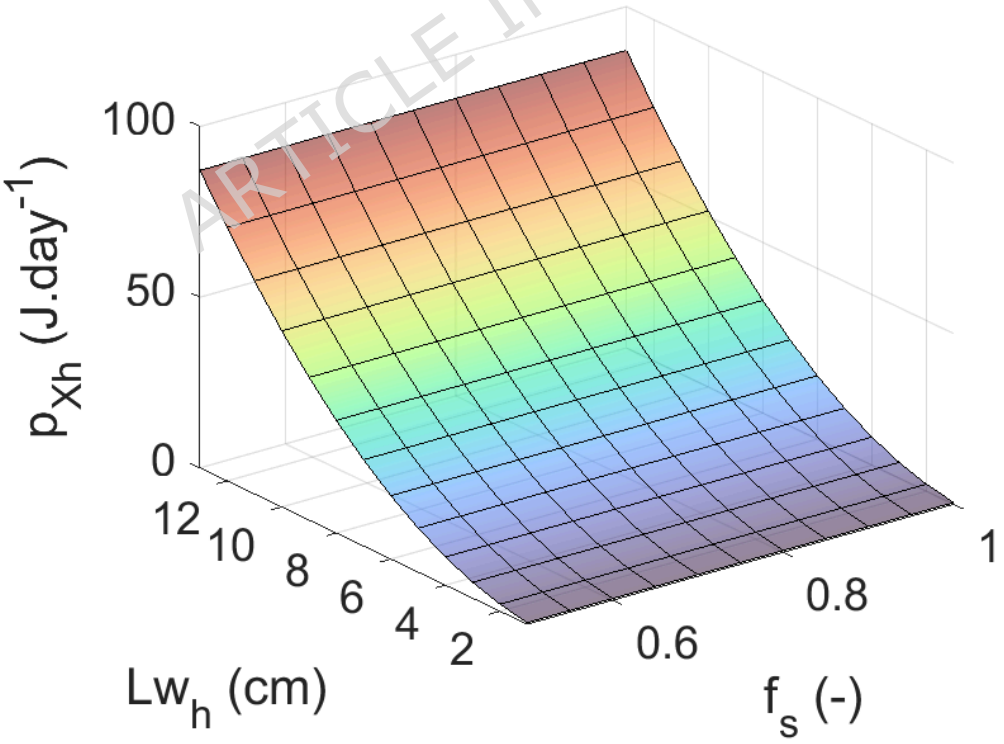

(b)

Figure 2. Modeled ingestion fluxes with *Christineconcha regab* farming dynamic energy budget model. (a) symbiont ingestion ($\dot{p}_{Xs}$) and (b) host ingestion flux ($\dot{p}_{Xh}$) as a function of symbiont functional response (f_s) and host shell length (Lw_h) modeled with *Christineconcha regab* farming model (host functional response f_h = 0.18 ; T = 2.55°C).

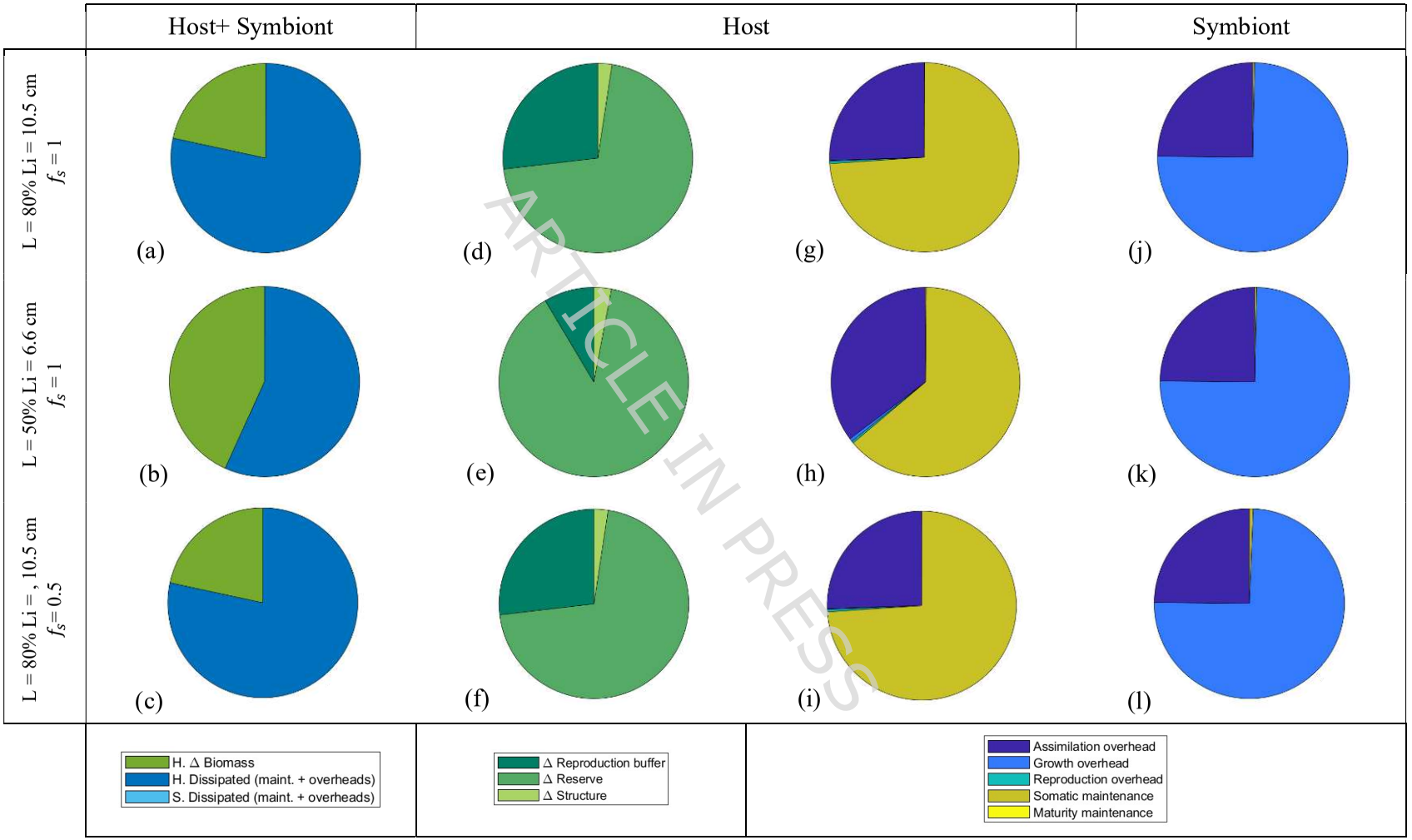

Figure 3. Energy distribution ($J d^{-1}$) within *Christineconcha regab* and its sulfur-oxidizing symbiont population using the farming model (temperature T = 2.55°C, host functional response $f_h = 0.18$). *L*, *C. regab* shell length (cm); L_i, maximum shell length estimated by the model ($L_i = 13.15$ cm); f_s, symbiont functional response (-); Δ, variation ($J d^{-1}$).

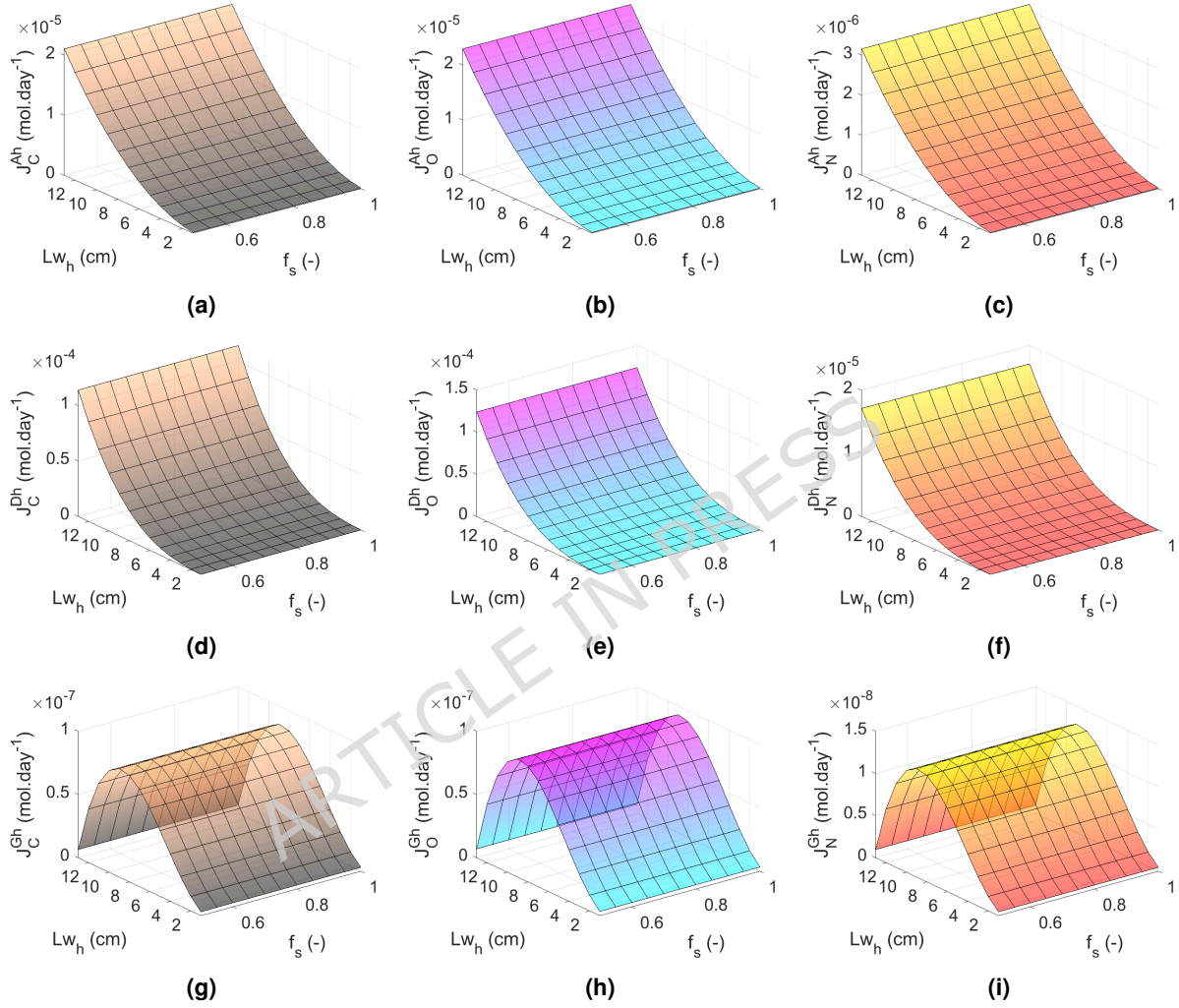

Figure 4. Host *Christineconcha regab* modeled chemical element (carbon, oxygen and nitrogen) fluxes with the farming dynamic energy budget model of assimilation, dissipation and growth transformations as a function of *C. regab* shell length (Lw_h) and symbiont functional response (f_s). (a,b,c), host assimilated fluxes of carbon, oxygen and nitrogen, respectively; (d,e,f), host dissipated flux of carbon, oxygen and nitrogen, respectively; (g,h,i), host flux for growth of carbon, oxygen and nitrogen, respectively. J, fluxes (mol d^{-1}); Ah, host assimilation; Dh, host dissipation; Gh, host growth; C, carbon; O, oxygen; N, nitrogen. A color gradient was applied to interpolated values of chemical fluxes (J), from the lowest to the highest values.

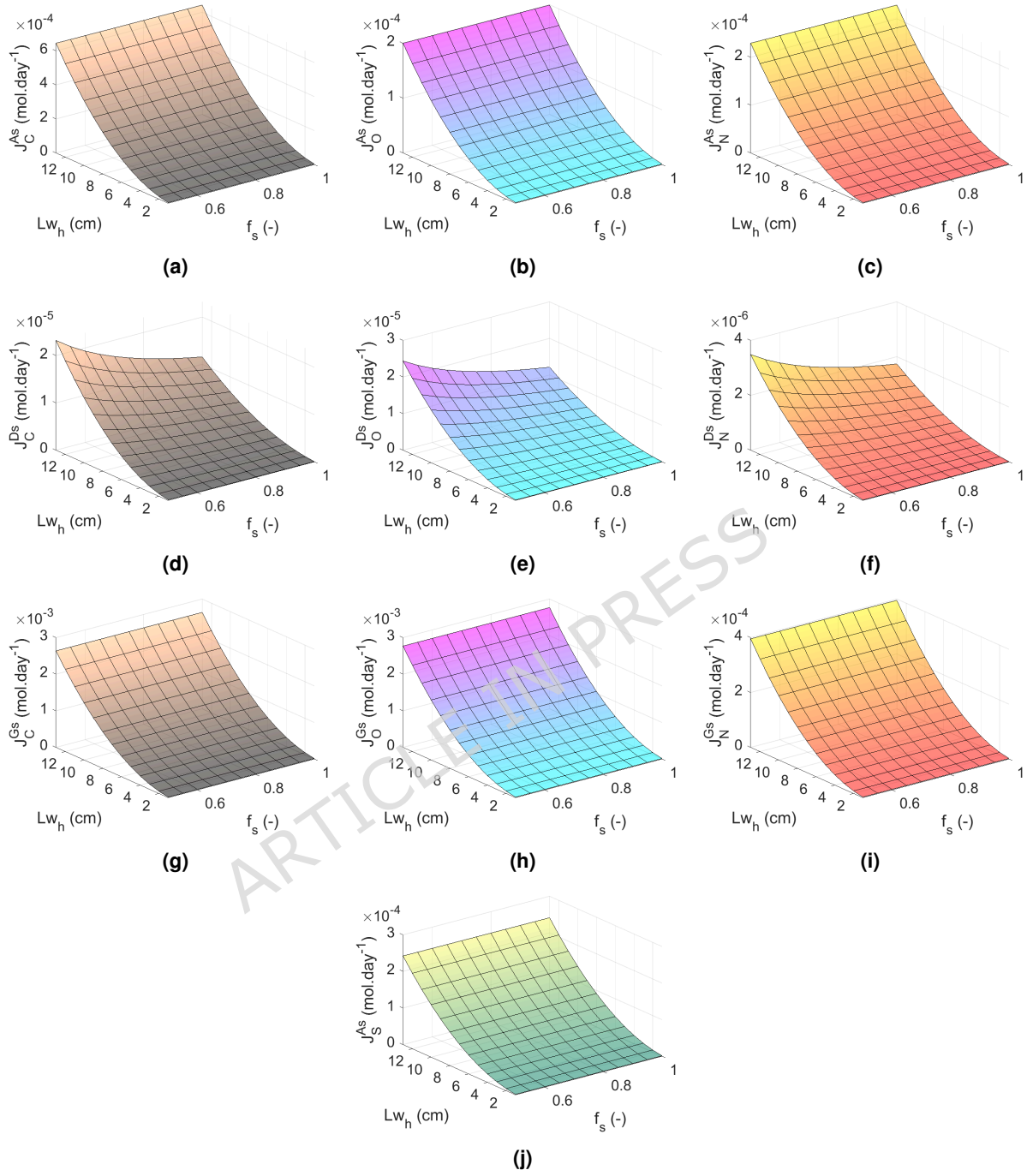

Figure 5. *Christineconcha regab* symbionts modeled chemical element (carbon, oxygen, nitrogen and sulfur) fluxes with the farming dynamic energy budget model of assimilation, dissipation and growth transformations as a function of *C. regab* shell length (Lw_h) and symbionts functional response (f_s). (a,b,c), symbiont assimilated fluxes of carbon, oxygen and nitrogen, respectively; (d,e,f), symbiont dissipated flux of carbon, oxygen and nitrogen, respectively; (g,h,i), symbiont flux for growth of carbon, oxygen and nitrogen, respectively; (j) symbiont assimilated flux of sulfur. J, fluxes (mol d^{-1}); As, symbiont assimilation; Ds, symbiont dissipation; Gs, symbiont growth; C, carbon; O, oxygen; N, nitrogen; S, sulfur. A color gradient was applied to interpolated values of chemical fluxes (J), from the lowest to the highest values.

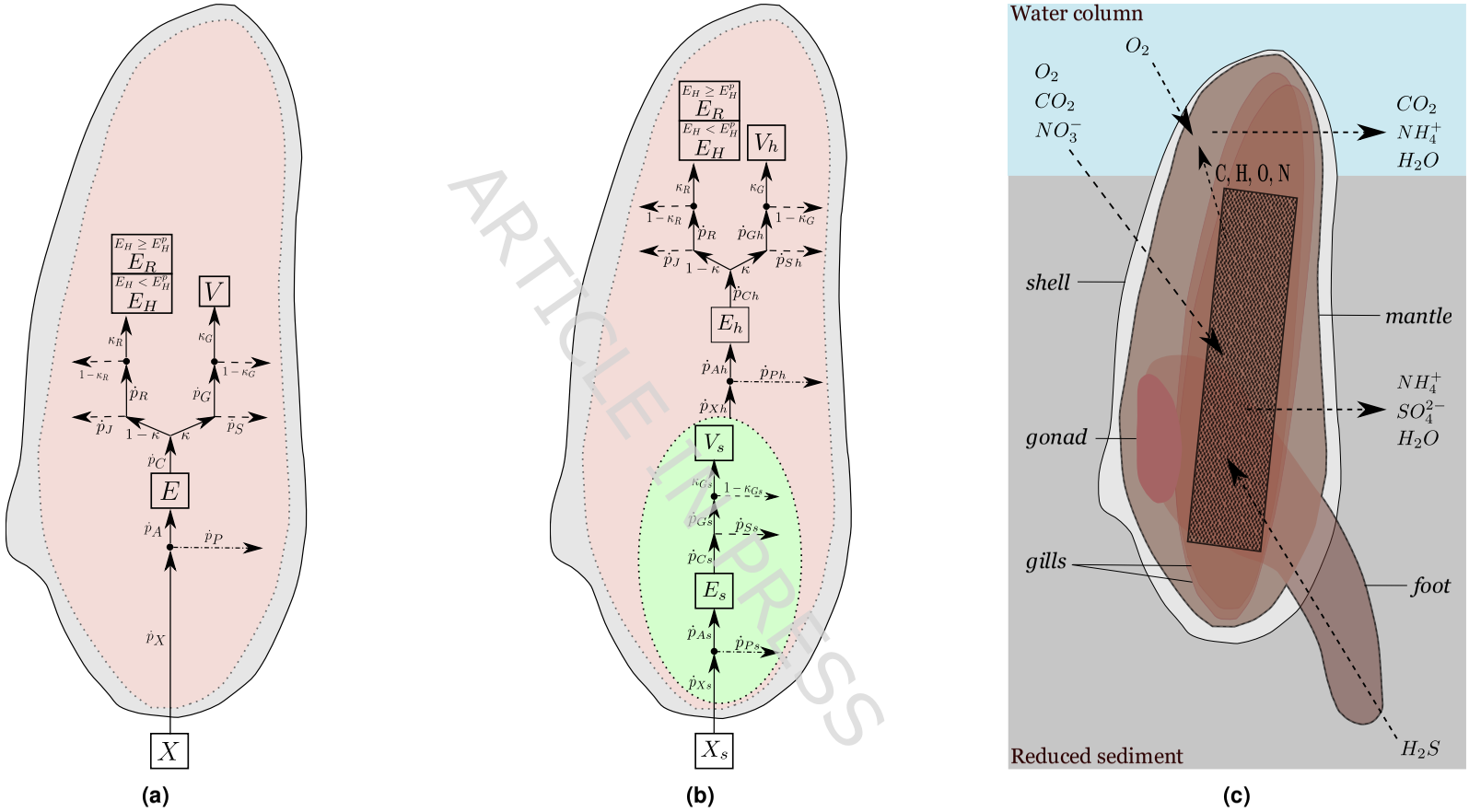

Figure 6. *Christineconcha regab* dynamic energy budget modeling schemes: (a) classical abj model, (b) farming model. (c) Chemicals fluxes between *Christineconcha regab* and its sulfur-oxidizing symbionts and their environment. (a,b) Plain line text box: state variables; Arrow: energy fluxes $\dot{p}$ ($\mathrm{J\,d^{-1}}$); Dotted line: boundaries of the models; green background: sulfur-oxidizing symbionts; red background: bivalve host soft body; grey background: bivalve host shell. Chemicals fluxes between *Christineconcha regab* and its sulfur-oxidizing symbionts and their environment. (c) Black box: sulfur-oxidizing symbionts; dashed arrows: chemical fluxes.

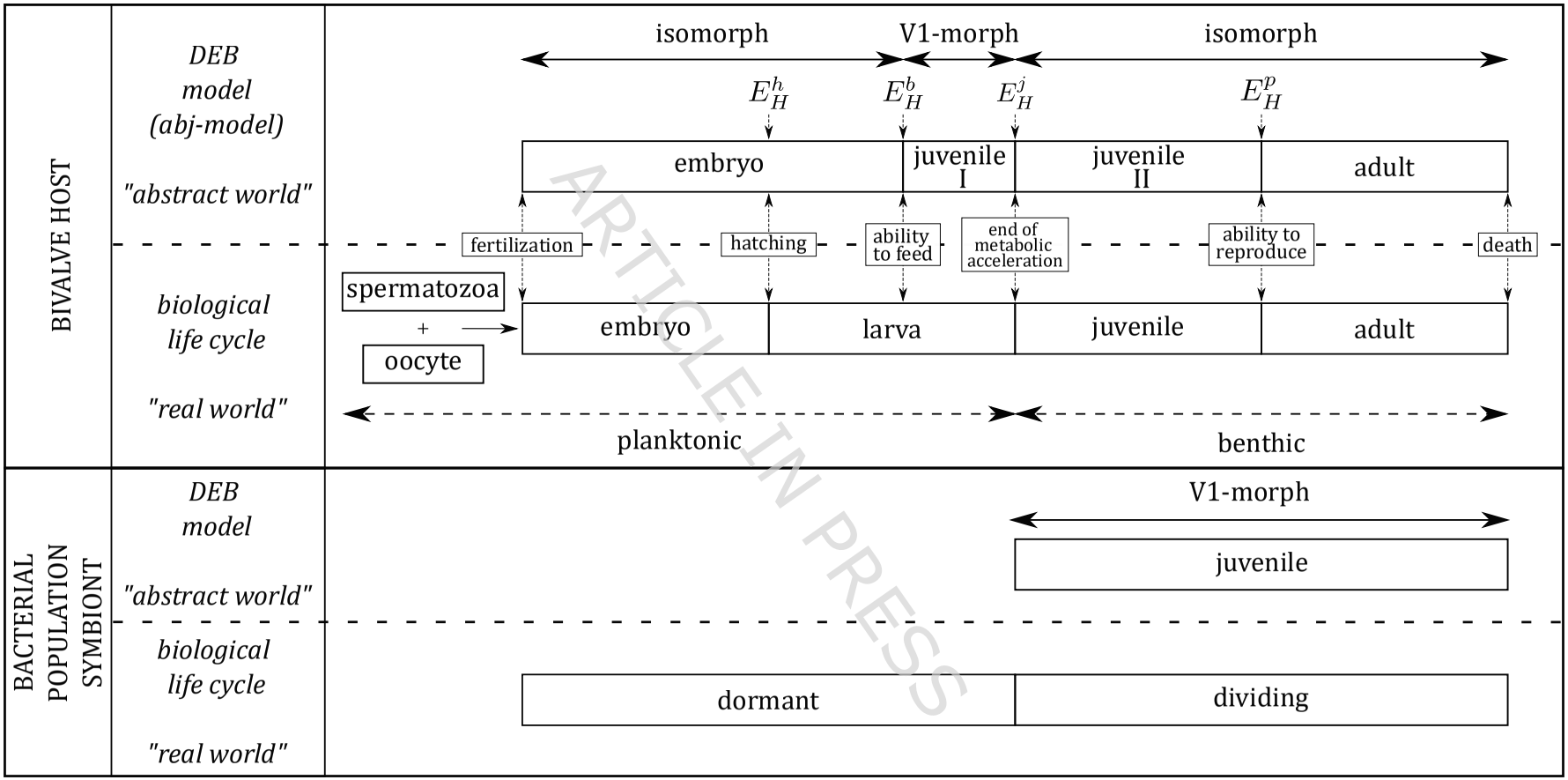

Figure 7. The "real world" representation of the biological life cycle versus the "abstract world" of the dynamic energy budget (DEB) theory on the different life stages of *Christineconcha regab* and its sulfur-oxidizing symbionts. E_H^b, host maturity level at birth (J) ; E_H^h, host maturity level at hatching (J) ; E_H^j, host maturity level at metamorphosis (J) ; E_H^p, host maturity level at puberty (J). “Juvenile II” stage corresponds to a juvenile in a biological sense whereas “juvenile I” corresponds to a larval stage.

Table 1. Classical dynamic energy budget model state variables and fluxes. s_M was defined in Table 2 and model parameters were defined in Table 3. E_H^p, maturity level at puberty (J); E_H^b, maturity level at birth (J); f, functional response (-); $\dot{k}_J$, maturity maintenance rate coefficient (-); $\{\dot{p}_{Xmh}\}$, max specific feeding power ($\mathrm{J\,d^{-1}\,cm^2}$).

State variable	Definition	Unit	Formula
E	reserve	J	$\frac{\mathrm{d}E}{\mathrm{d}t} = \dot{p}_A - \dot{p}_C$
V	structure	cm^3	$\frac{\mathrm{d}V}{\mathrm{d}t} = \frac{\dot{p}_G}{[E_G]}$
E_H	maturity	J	$\frac{\mathrm{d}E_H}{\mathrm{d}t} = \dot{p}_R$ if $E_H < E_H^p$
			$\frac{\mathrm{d}E_H}{\mathrm{d}t} = 0$ otherwise
E_R	reproduction buffer	J	$\frac{\mathrm{d}E_R}{\mathrm{d}t} = 0$ if $E_H < E_H^p$
			$\frac{\mathrm{d}E_R}{\mathrm{d}t} = \kappa_R \dot{p}_R$ otherwise

Flux	Definition	Unit	Formula
$\dot{p}_X$	$\mathrm{J\,d^{-1}}$	ingestion	$\{\dot{p}_{Xm}\} f V^{2/3} = \frac{\dot{p}_A}{\kappa_X}$, when $E_H \geq E_H^b$
$\dot{p}_A$	$\mathrm{J\,d^{-1}}$	assimilation	$\{\dot{p}_{Am}\} s_M f V^{2/3}$
$\dot{p}_P$	$\mathrm{J\,d^{-1}}$	faecation	$(1-\kappa_p)\dot{p}_X$
$\dot{p}_C$	$\mathrm{J\,d^{-1}}$	reserve mobilization	$E \frac{\dot{v} s_M [E_G] V^{2/3} + \dot{p}_S}{\kappa E + [E_G] V}$
$\dot{p}_S$	$\mathrm{J\,d^{-1}}$	somatic maintenance	$[\dot{p}_M] V$
$\dot{p}_G$	$\mathrm{J\,d^{-1}}$	growth	$\kappa \dot{p}_C - \dot{p}_S$
$\dot{p}_J$	$\mathrm{J\,d^{-1}}$	maturity maintenance	$\dot{k}_J E_H$
$\dot{p}_R$	$\mathrm{J\,d^{-1}}$	maturation and reproduction	$(1-\kappa)\dot{p}_C - \dot{p}_J$

Table 2. Acceleration coefficient (s_M) to model metabolic acceleration in the classical and farming dynamic energy budget models. E_H, level of maturity (J); E_H^b, level of maturity at birth (J); E_H^j, level of maturity at metamorphosis (J); E_H^p, level of maturity at puberty (J); L_b, structural length at birth (cm); L_j structural length at metamorphosis (cm)[36].

Maturity level (E_H)	s_M
$E_H < E_H^b$ (embryo)	$\frac{L_b}{L_b} = 1$
$E_H^b \leq E_H < E_H^j$ (early juvenile)	$\frac{L}{L_b}$
$E_H^j \leq E_H$ (late juvenile + adult)	$\frac{L_j}{L_b} = s_M$

Table 3. Parameters of *Christineconcha regab* classical and farming dynamic energy budget models. h., host; sb., symbionts.

Model	Notation	Description	Unit
Classical	z	zoom factor	-
	κ_X	digestion efficiency of food to reserve	-
	κ_P	faecation efficiency of food to faeces	-
	$\dot{v}$	energy conductance	$\mathrm{cm\,d^{-1}}$
	κ	allocation fraction to soma	-
	κ_R	reproduction efficiency	-
	$[\dot{p}_M]$	volume-specific somatic maintenance cost	$\mathrm{J\,d^{-1}\,cm^3}$
	$\dot{k}_J$	maturity maintenance rate coefficient	$\mathrm{d^{-1}}$
	$[E_G]$	specific cost for structure	$\mathrm{J\,cm^{-3}}$
	E_H	maturity at hatching	J
	E_H^b	maturity at birth	J
	E_H^j	maturity at metamorphosis	J
	E_H^p	maturity at puberty	J
	$\ddot{h}_a$	Weibull aging acceleration	$\mathrm{d^{-2}}$
	s_G	Gompertz stress coefficient	-
	δ_M	shape coefficient	-
	δ_{Me}	shape coefficient of larva	-
Farming	z_h	h. zoom factor	-
	κ_{Xh}	h. digestion efficiency of food to reserve	-
	κ_{Ph}	h. faecation efficiency of food to feces	-
	$\dot{v}_h$	h. energy conductance	$\mathrm{cm\,d^{-1}}$
	κ_h	h. allocation fraction to soma	-
	κ_{Rh}	h. reproduction efficiency	-
	$[\dot{p}_{Mh}]$	h. volume-specific somatic maintenance cost	$\mathrm{J\,d^{-1}\,cm^3}$
	$\dot{k}_{Jh}$	h. maturity maintenance rate coefficient	$\mathrm{d^{-1}}$
	$[E_{Gh}]$	h. specific cost for structure	$\mathrm{J\,cm^{-3}}$
	E_{Hh}^h	h. maturity at hatching	J
	E_{Hh}^b	h. maturity at birth	J
	E_H^{jh}	h. maturity at metamorphosis	J
	E_{Hh}^p	h. maturity at puberty	J
	$\ddot{h}_{ah}$	h. Weibull aging acceleration	$\mathrm{d^{-2}}$
	s_{Gh}	h. Gompertz stress coefficient	-
	δ_{Mh}	h. shape coefficient	-
	δ_{Meh}	h. shape coefficient of larva	-
	vks	h. half saturation coefficient	-
	$[\dot{p}_{Ams}]$	sb. maximum assimilation rate	$\mathrm{J\,d^{-1}\,cm^{-2}}$
	κ_{Xs}	sb. digestion efficiency of food to reserve	-
	κ_{Ps}	sb. excretion efficiency of food to excretes	-
	$\dot{k}_{Es}$	sb. specific-energy conductance	$\mathrm{d^{-1}}$
	$[\dot{p}_{Ms}]$	sb. volume-specific somatic maintenance cost	$\mathrm{J\,d^{-1}\,cm^3}$
	$[E_{Gs}]$	sb. specific cost for structure	$\mathrm{J\,cm^{-3}}$
	δ_{MVs}	sb. shape coefficient of structure	-
	Y_{SE}^{As}	sb. H_2S assimilation yield per C-mol of reserve	H_2S mol C-mol^{-1}
	Y_{HE}^{As}	sb. H_2O assimilation yield per C-mol of reserve	H_20 mol C-mol^{-1}

Table 4. *Christineconcha regab* farming model state variables and energy fluxes. h, host; sb, symbionts. s_M was defined in Table 2 and model parameters were defined in Table 3. E_{Hh}^p, host maturity level at puberty (J); E_{Hh}^b, host maturity level at birth (J); f_h, host functional response (-); f_s, symbiont functional response (-); $\dot{k}_{Jh}$, host maturity maintenance rate coefficient (-); $[\dot{p}_{Xms}]$, symbiont max specific feeding power ($\mathrm{J\,d^{-1}\,cm^3}$).

State variable	Description	Unit	Formula
E_h	h. reserve	J	$\frac{\mathrm{d}E_h}{\mathrm{d}t} = \dot{p}_{Ah} - \dot{p}_{Ch}$
V_h	h. structure	$\mathrm{cm^3}$	$\frac{\mathrm{d}V_h}{\mathrm{d}t} = \frac{\dot{p}_{Gh}}{[E_{Gh}]}$
E_{Hh}	h. maturity	J	$\frac{\mathrm{d}E_{Hh}}{\mathrm{d}t} = \dot{p}_{Rh}$ if $E_{Hh} < E_{Hh}^p$
			$\frac{\mathrm{d}E_{Hh}}{\mathrm{d}t} = 0$ otherwise
E_{Rh}	h. reproduction buffer	J	$\frac{\mathrm{d}E_{Rh}}{\mathrm{d}t} = 0$ if $E_{Hh} < E_{Hh}^p$
			$\frac{\mathrm{d}E_R}{\mathrm{d}t} = \kappa_R \dot{p}_R$ otherwise
E_s	sb. reserve	J	$\frac{\mathrm{d}E_s}{\mathrm{d}t} = \dot{p}_{As} - \dot{p}_{Cs} - \dot{p}_{XEh}$
V_s	sb. structure	$\mathrm{cm^3}$	$\frac{\mathrm{d}V_s}{\mathrm{d}t} = \frac{\dot{p}_{Gs}}{[E_{Gs}]} - \frac{\dot{p}_{XV}}{[E_{Vs}]}$

Flux	Description	Unit	Formula
$\dot{p}_{Xh}$	h. ingestion	$\mathrm{J\,d^{-1}}$	$\dot{p}_{XEh} + \dot{p}_{XVh}$ when $E_{Hh} \geq E_{Hh}^b$
$\dot{p}_{XEh}$	h. ingestion of sb. reserve E_s	$\mathrm{J\,d^{-1}}$	$\gamma \dot{p}_{Xh} = \frac{E_s}{E_{Vs}} \dot{p}_{XVh}$
$\dot{p}_{XVh}$	h. ingestion of sb. structure V_s	$\mathrm{J\,d^{-1}}$	$(1-\gamma)\dot{p}_{Xh} = \frac{E_{Vs}}{E_s} \dot{p}_{XEh}$
$\dot{p}_{Ah}$	h. assimilation	$\mathrm{J\,d^{-1}}$	$\{\dot{p}_{Amh}\} s_M f_h V_h^{2/3}$
$\dot{p}_{Ph}$	h. faecation	$\mathrm{J\,d^{-1}}$	$(1-\kappa_{ph})\dot{p}_{Xh}$
$\dot{p}_{Ch}$	h. reserve mobilization	$\mathrm{J\,d^{-1}}$	$E_h \frac{\dot{v}_h s_M [E_{Gh}] V_h^{2/3} + \dot{p}_{Sh}}{\kappa_h E_h + [E_{Gh}] V_h}$
$\dot{p}_{Sh}$	h. somatic maintenance	$\mathrm{J\,d^{-1}}$	$[\dot{p}_{Mh}] V_h$
$\dot{p}_{Gh}$	h. growth	$\mathrm{J\,d^{-1}}$	$\kappa_h \dot{p}_{Ch} - \dot{p}_{Sh}$
$\dot{p}_{Jh}$	h. maturity maintenance	$\mathrm{J\,d^{-1}}$	$\dot{k}_{jh} E_{Hh}$
$\dot{p}_{Rh}$	h. maturation and reproduction	$\mathrm{J\,d^{-1}}$	$(1-\kappa_h)\dot{p}_{Ch} - \dot{p}_{Jh}$
$\dot{p}_{Xs}$	sb. ingestion	$\mathrm{J\,d^{-1}}$	$[\dot{p}_{Xms}] f_s V_s$
$\dot{p}_{As}$	sb. assimilation	$\mathrm{J\,d^{-1}}$	$[\dot{p}_{Ams}] f_s V_s$
$\dot{p}_{Ps}$	sb. excretion	$\mathrm{J\,d^{-1}}$	$(1-\kappa_{ps})\dot{p}_{Xs}$
$\dot{p}_{Cs}$	sb. mobilization	$\mathrm{J\,d^{-1}}$	$E_s \frac{\dot{k}_{Es} V_s [E_{Gs}] + \dot{p}_{Ss}}{E_s + [E_{Gs}] V_s}$
$\dot{p}_{Ss}$	sb. somatic maintenance	$\mathrm{J\,d^{-1}}$	$[\dot{p}_{Ms}] V_s$
$\dot{p}_{Gs}$	sb. growth	$\mathrm{J\,d^{-1}}$	$\dot{p}_{Cs} - \dot{p}_{Ss}$